SUPPLEMENTARY INFORMATION

Unveiling Mechanistic Patterns of Copper-Catalyzed Radical Bond Formation through Linear Free Energy Relationship

Guo-Xiong Xu,[1,5] Ji-Ren Liu,[1,5] Zeng Gao,[2,5] Miao-Jiong Tang,[1] Yi-Zhou Sun,[1] Zhong-Liang Li,[2] Xin-Yuan Liu,[3] Shuo-Qing Zhang,[1]* Xin Hong[1,4]*

[1]Center of Chemistry for Frontier Technologies, Department of Chemistry, State Key Laboratory of Clean Energy Utilization, Zhejiang University, Hangzhou, China

[2]Dongguan Key Laboratory of Interdisciplinary Science for Advanced Materials and Large Scale Scientific Facilities, School of Physical Sciences, Great Bay University, Dongguan, China

[3]Shenzhen Grubbs Institute, Department of Chemistry and Guangming Advanced Research Institute, Southern University of Science and Technology, Shenzhen, China

[4]School of Chemistry and Chemical Engineering, Henan Normal University, China

[5]These authors contributed equally

TABLE OF CONTENTS

1 Computational Details

1.1 Computational Methods.

All density functional theory (DFT) calculations were performed using Gaussian 16 program[1].

Geometry optimizations were employed with B3LYP functional[2,3], with the D3 version of Grimme's dispersion corrections[4] and Becke-Johnson damping[5]. And LANL2DZ basis set[6-9] was applied for copper, bromine and iodine, and 6-31G(d) basis set was used for other atoms. Frequency analysis was also performed at the same level of theory as geometry optimization to confirm optimized stationary points were either local minimum or transition state, as well as to evaluate zero-point vibrational energies and thermal corrections for enthalpies and free energies at 298.15 K.

Single-point energies were evaluated with B3LYP functional[2,3] with D3 version of Grimme's dispersion corrections[4] with Becke-Johnson damping[5]. SDD basis set[6,10-12] was used for copper, bromine and iodine, and 6-311+G(d,p) basis set was used for other atoms. The solvation energies (if mentioned) were calculated with a self-consistent reaction field (SCRF) using the SMD implicit solvent model[13].

Also, we calculated the single point energies at DLPNO-CCSD(T)/def2-TZVP level of theory to further evaluate the accuracy of the computation protocol. The DLPNO-CCSD(T)[14] calculation is performed with ORCA 5.0.4[15,16]. Def2-TZVP[17] basis set and corresponding auxiliary basis set def2-TZVP/C [18] were employed for all atoms. UHF (unrestricted Hartree-Fock) reference wavefunctions were used for all computed species. "TightPNO" and "TightSCF" criteria were also used. "UseFullLMP2Guess" option in MDCI module of ORCA was set to "FALSE" in order to compare the energies of closed-shell and open-shell species in "TightPNO" calculations.

To correct the Gibbs free energies under 1 atm to the standard state in solution (1 mol/L), a correction of $RT\ln(c_s/c_g)$ is added to energies of all species. c_s stands for the standard molar concentration in solution (1 mol/L), c_g stands for the standard molar concentration in gas phase (about 0.040876 mol/L), and R is the gas constant. For calculated intermediates at the standard state of 1 mol/L at 298.15 K, the correction value equaling to 1.89 kcal/mol was used.

The 3D diagrams of optimized structures shown in the main text and below here in supplementary information for computations were generated with CYLview software[19].

1.2 Workflow for Locating TS.

Supplementary Figure 1 provides a detailed illustration of the workflow for locating transition states in reductive elimination (RE), radical substitution (RS), and ion pair-type bond formation (IP) processes for ligand-radical-nucleophile combinations.

Step 1: Set the spin multiplicity to 1 (singlet) and construct a Cu(III) complex with coordinated ligand, radical, and nucleophile.

Step 1.2: Fix the bond lengths of Cu–R, Cu–Nu, and R–Nu to appropriate values (typically 2.1–2.3 Å) for optimization, based on the structural characteristics of the RE transition state. Release the constraints and re-optimize to obtain the accurate RE-TS structure.

Step 1.2.1: Perform a wavefunction stability check on the RE-TS. If unstable, recalculate a stable open-shell singlet (OSS) wavefunction and re-optimize the structure for the RS-TS.

Step 1.3: If Cu–R bond dissociation occurs during the RE-TS search (Cu–R distance > 2.5 Å), optimize the structure to obtain an ion pair consisting of a Cu(I) complex and the corresponding radical cation.

Step 1.3.1: Fix the R–Nu bond length to an appropriate value (typically 2.1–2.4 Å) for optimization. Release the constraints and re-optimize to obtain the accurate IP-TS structure.

Step 1.3.1.1: Perform a wavefunction stability check on the IP-TS. If unstable, recalculate a stable OSS wavefunction and re-optimize the structure for the RS-TS.

Step 1.4: Perform a wavefunction stability check on the Cu(III) complex. If unstable, recalculate a stable OSS wavefunction to obtain the van der Waals complex of the Cu(II) complex and the radical.

Step 2: Set the spin multiplicity to 3 (triplet) and construct a van der Waals complex composed of a Cu(II) complex with coordinated

ligands and a nucleophile, along with an unbonded radical.

Step 2.1: Break the spin symmetry of the triplet van der Waals complex by changing the spin multiplicity to 1 (singlet) and obtain an OSS wavefunction. Optimize the structure to obtain an OSS van der Waals complex.

Step 2.1.1: If the van der Waals complex has a stable closed-shell singlet (CSS) wavefunction, re-optimize the structure to obtain an ion pair consisting of a Cu(I) complex and the corresponding radical cation.

Step 2.1.2: Fix the R–Nu bond length to an appropriate value (typically ~2.2 Å) for optimization. Release the constraints and re-optimize to obtain the accurate RS-TS structure.

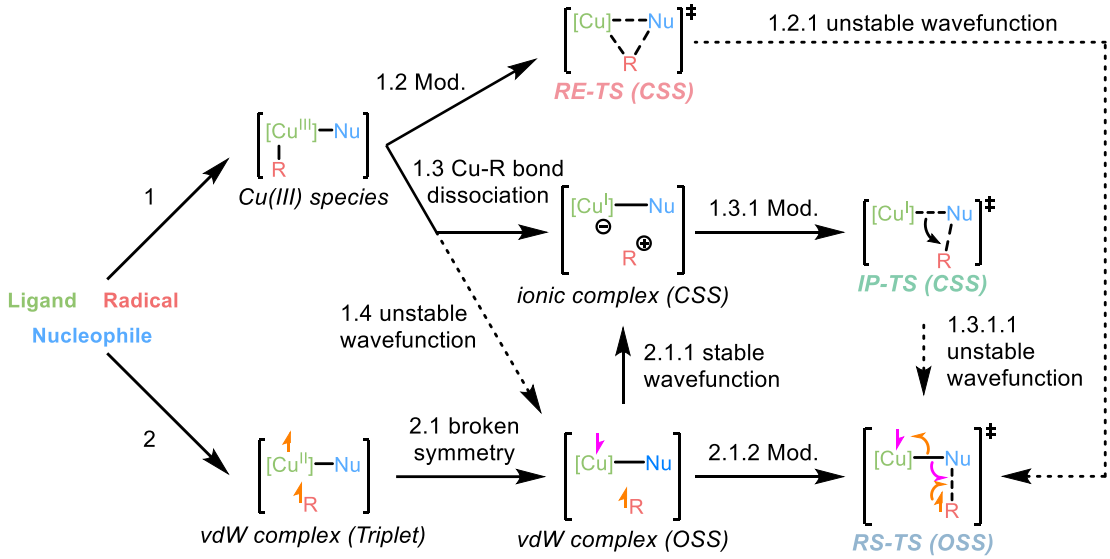

Supplementary Figure 1: Workflow for locating transition states of reductive elimination (RE-TS), radical substitution (RS-TS), and ion pair-type bond formation (IP-TS). "Broken symmetry" step: Transition from triplet to singlet spin states while keeping atomic coordinates fixed. "Mod." step (modredundant): Optimization with key bond lengths (forming and breaking) constrained to transition state-like distances. Abbreviations: RE, reductive elimination; RS, radical substitution; IP, ion pair-type bond formation; TS, transition state; CSS, closed-shell singlet; OSS, open-shell singlet.

1.3 Conformation Search.

We systematically examined the conformational factors associated with the catalytic system. For each reaction, we constructed a comprehensive set of initial guess structures and performed geometry optimizations. Among the optimized conformers, the lowest-energy structure was consistently chosen as the representative for subsequent analysis.

To make our conformational search workflow more transparent, we included a representative case study involving a flexible substrate combination (Supplementary Figure 2). In this example, we first considered conformational factors from the nucleophile and radical individually: the vinyl fragment of the nucleophile has two key orientations, while the α-naphthyl radical features two distinct conformers due to ring orientation. The ligand is a rigid tridentate system and thus does not introduce additional conformational complexity at the transition state.

When combining the radical and nucleophile, the bond formation region relative to the LCu(II) catalyst can adopt two possible orientations along the z-axis. In addition, the radical can freely rotate around the Cu–C bond, leading to three further relative orientations. Together, this introduced six additional conformational possibilities. When combined with the intrinsic conformers of the radical and nucleophile, a total of 6 × 2 × 2 = 24 initial transition state guesses were generated. Optimizations of these structures yielded 24 transition states (Supplementary Figure 3 and Supplementary Table 1), from which the lowest-energy TS-17 was selected for inclusion in the LFER

analysis.

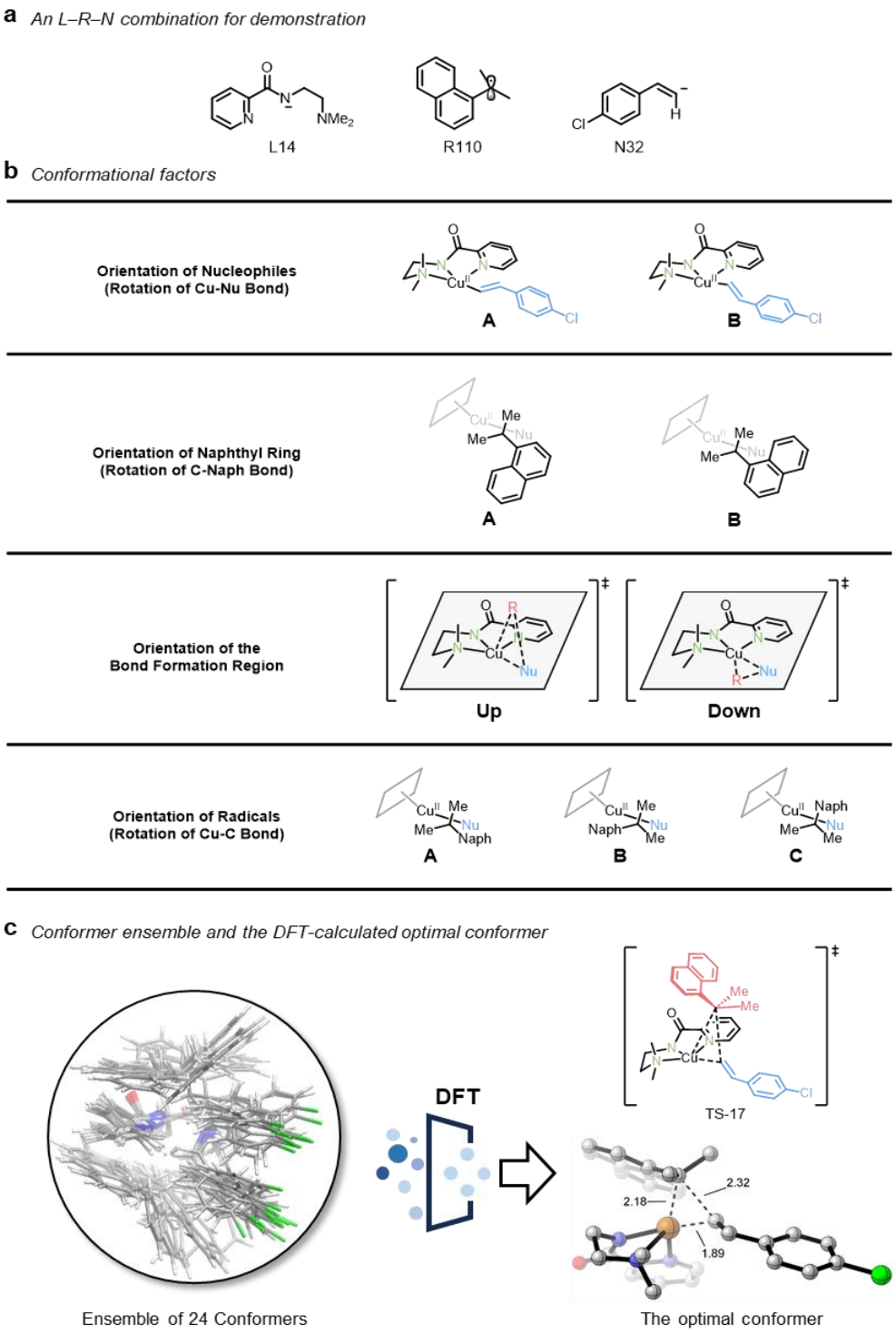

Supplementary Figure 2: a Representative conformational search for a flexible substrate combination, showing the selected system. **b** Key conformational factors considered. **c** The resulting ensemble of 24 conformers with the DFT-optimized lowest-energy transition state structure.

Supplementary Figure 3 displays the 3D molecular structures of the 24 conformations composed of these conformational factors.

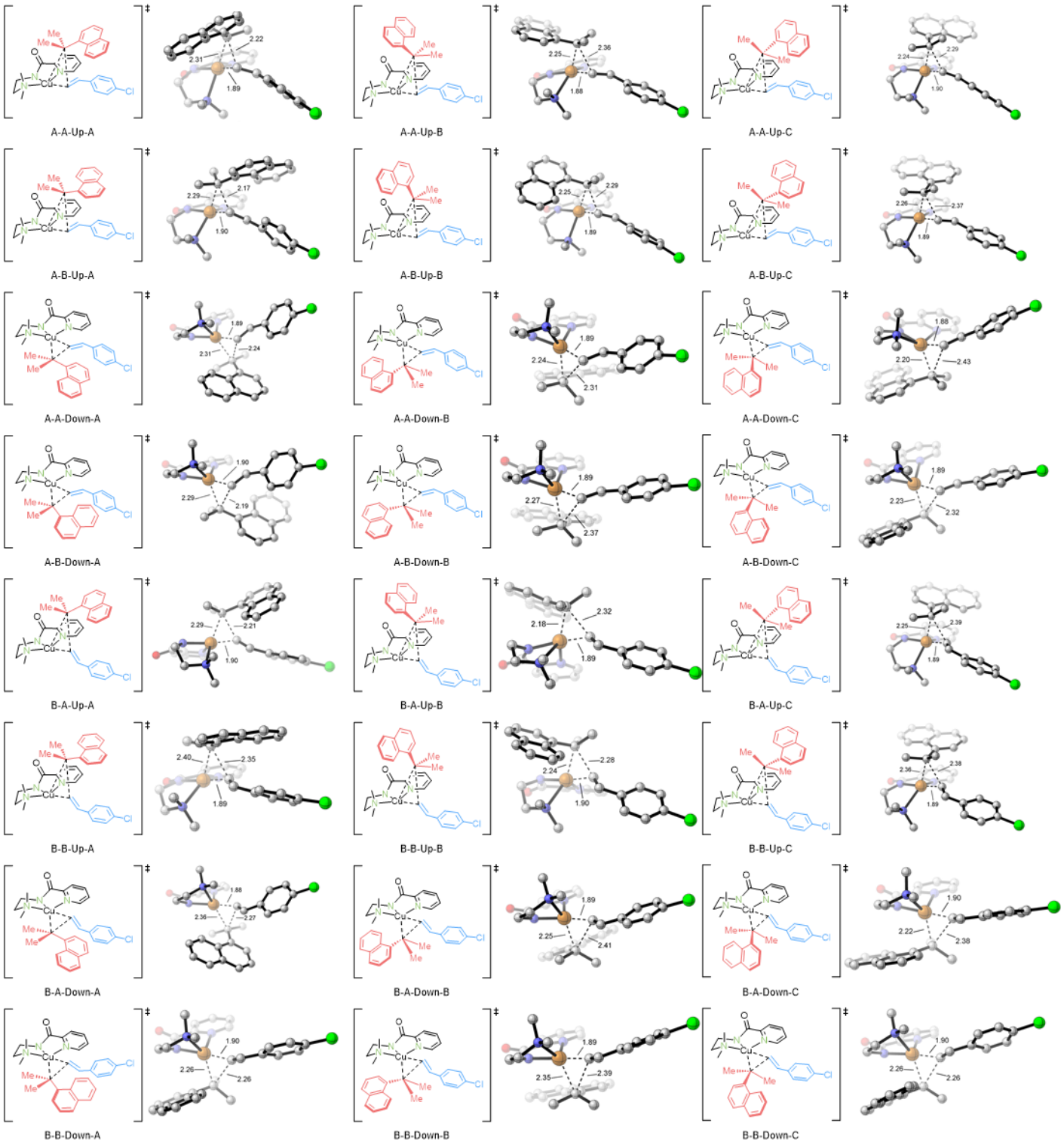

Supplementary Figure 3: Molecular structures composed of conformational factors. Hydrogen atoms are omitted for clarity.

Supplementary Table 1: Summary of the 24 initial transition state conformers generated for the representative case and corresponding optimization results.

No	Conformations of Nucleophile	Conformations of Radical	Bond Formation Orientations	Radical Rotations	$\Delta\Delta G^{\ddagger}$ (kcal/mol)
TS-1	A	A	Down	A	5.2
TS-2	A	A	Down	B	4.4
TS-3	A	A	Down	C	1.4
TS-4	A	A	Up	A	3.8
TS-5	A	A	Up	B	4.9
TS-6	A	A	Up	C	1.9
TS-7	A	B	Down	A	1.7
TS-8	A	B	Down	B	4.7
TS-9	A	B	Down	C	3.1
TS-10	A	B	Up	A	5.2
TS-11	A	B	Up	B	1.9
TS-12	A	B	Up	C	4.1
TS-13	B	A	Down	A	6.2
TS-14	B	A	Down	B	3.2
TS-15	B	A	Down	C	3.2
TS-16	B	A	Up	A	6.4
TS-17 (Optimal)	B	A	Up	B	0.0
TS-18	B	A	Up	C	2.2
TS-19	B	B	Down	A	4.5
TS-20	B	B	Down	B	1.6
TS-21	B	B	Down	C	5.9
TS-22	B	B	Up	A	8.9
TS-23	B	B	Up	B	4.3
TS-24	B	B	Up	C	6.1

2 Chemical Space

Supplementary Figure 4 provides the numbering of ligands. Supplementary Table 2 lists the LFER parameters of these ligands. Supplementary Table 3 lists their physicochemical properties and Supplementary Figure 5 show the corresponding distribution.

Supplementary Figure 6 provides the numbering of radicals. Supplementary Table 4 lists the LFER parameters of radicals. Supplementary Table 5 lists their physicochemical properties and Supplementary Figure 7 show the corresponding distribution.

Supplementary Figure 8 provides the numbering of nucleophiles. Supplementary Table 6 lists the LFER parameters of nucleophiles. Supplementary Table 7 lists their physicochemical properties and Supplementary Figure 9 show the corresponding distribution.

2.1 Ligands.

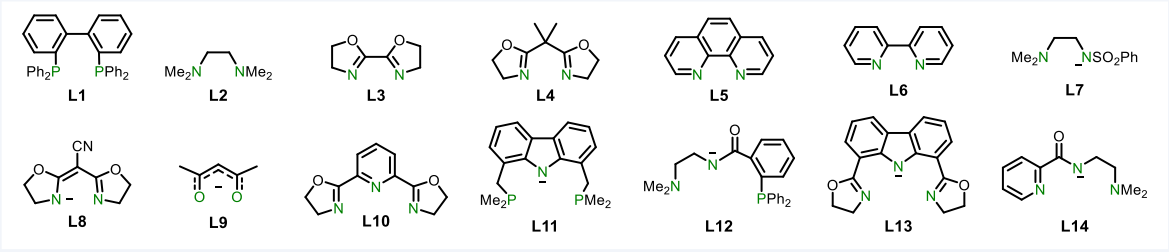

Supplementary Figure 4: Numbering of ligands involved in this study.

Supplementary Table 2: LFER parameters of ligands for RE, RS and IP processes.

Ligands	L_{RE}	L_{RS}	L_{IP}
L1	70.2	19.3	52.7
L2	87.0	40.5	64.9
L3	98.2	45.3	70.8
L4	80.0	35.1	54.6
L5	86.3	39.2	59.3
L6	83.7	40.3	56.6
L7	112.3	61.1	84.4
L8	120.2	69.8	88.8
L9	136.9	82.4	102.0
L10	67.0	16.6	40.6
L11	65.7	26.8	42.9
L12	79.0	38.5	53.7
L13	65.6	32.9	41.4
L14	88.4	52.0	58.0

Supplementary Table 3: Physicochemical properties of different ligand-coordinated Cu(II) complexes. E_{SOMO}, the energy of SOMO, values in kcal/mol. **BV(r=3),** the buried volume within a 3 Å radius of the copper center, values in %.

Ligands	E_{SOMO}	$BV(r=3)$
L1	–203.6	79.6
L2	–263.5	74.1
L3	–273.9	57.6
L4	–260.1	91.0
L5	–249.1	60.4
L6	–258.1	79.1
L7	–240.2	41.5
L8	–247.7	41.5
L9	–268.4	38.2

L10	–232.0	49.4
L11	–202.0	64.5
L12	–213.9	72.6
L13	–202.7	43.0
L14	–239.6	63.5

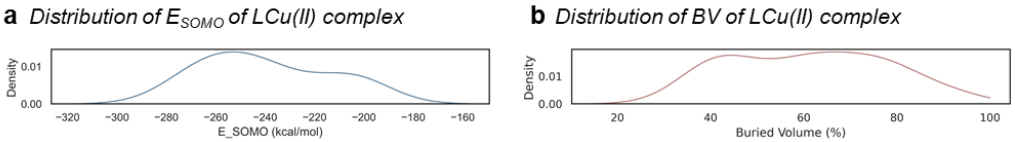

Supplementary Figure 5: Physicochemical property distribution of ligands.

2.2 Radicals.

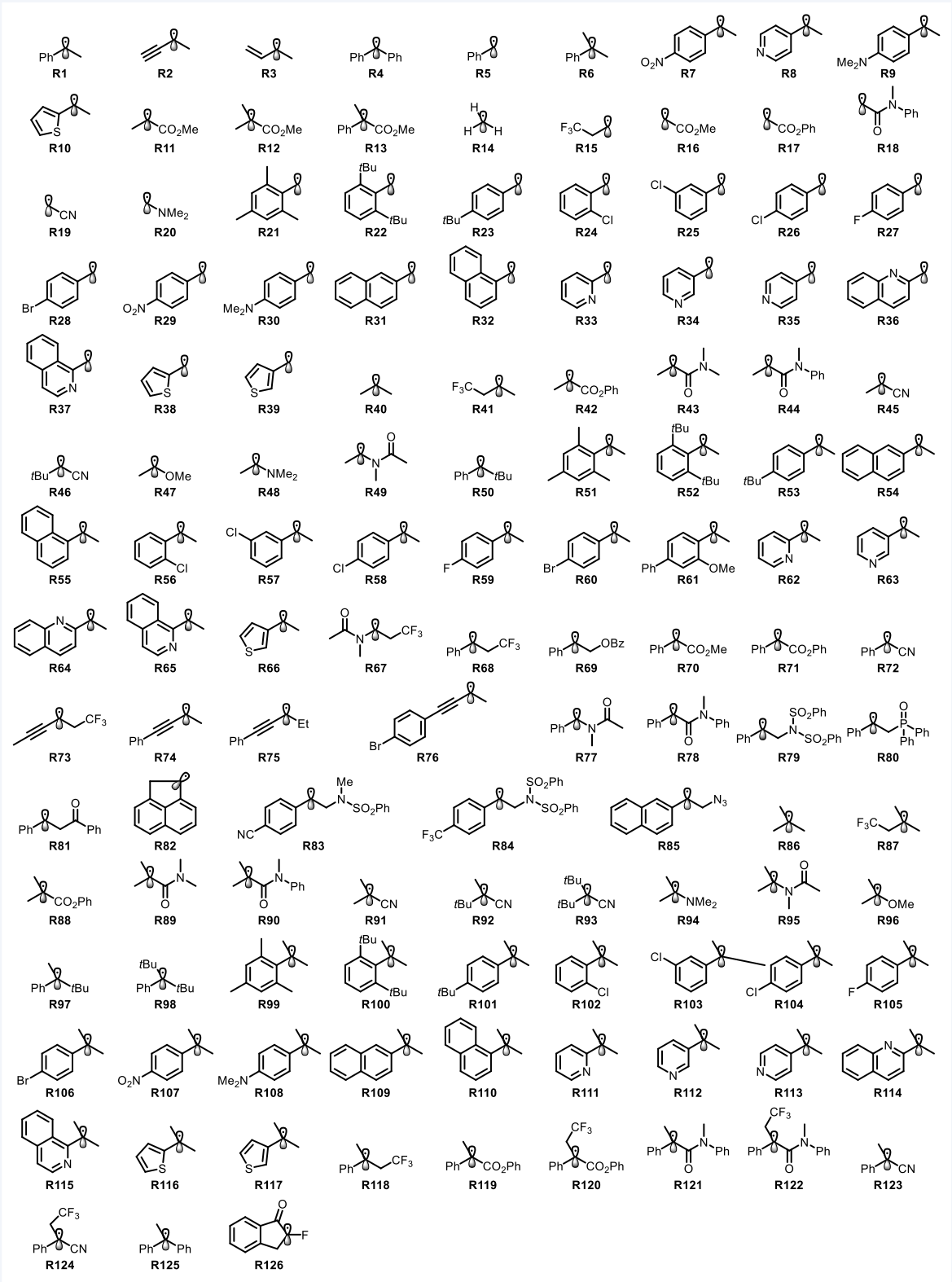

Supplementary Figure 6: Numbering of radicals involved in this study.

Supplementary Table 4: LFER parameters of radicals for RE, RS and IP processes. *, the corresponding ion pair-type bond formation transition states for these radicals could not be located. However, R_{IP} values for these radicals can be derived using multivariate linear regression (MLR), as shown in Section 5.2 and Supplementary Figure 16.

Radicals	R_{RE}	R_{RS}	R_{IP}
R1	46.4	9.6	49.6*
R2	44.8	5.6	47.1*
R3	41.9	4.3	47.1
R4	43.6	8.8	48.6
R5	50.4	9.7	50.9*
R6	39.5	9.2	48.6
R7	44.7	11.8	43.5*
R8	46.1	9.1	44.4*
R9	46.9	7.3	55.6
R10	43.0	6.8	49.4
R11	48.5	10.8	45.0*
R12	41.1	8.5	39.5*
R13	36.2	10.0	42.4*
R14	58.6	3.1	63.8*
R15	58.2	6.3	54.5*
R16	54.0	11.3	58.4*
R17	57.8	13.7	49.9*
R18	58.9	17.3	62.2*
R19	53.1	11.6	49.2*
R20	55.9	not located	73.5
R21	45.9	8.2	51.3*
R22	42.5	9.9	48.2*
R23	49.0	7.0	50.6*
R24	49.1	9.4	49.2*
R25	50.8	9.4	48.7*
R26	50.8	8.2	49.2*
R27	50.0	6.6	52.0*
R28	51.0	8.7	48.7*
R29	50.5	11.9	48.0*
R30	49.8	6.4	56.7
R31	50.4	9.1	50.4*
R32	49.7	10.2	50.8*
R33	52.5	9.4	50.2*
R34	50.8	9.1	49.6*

R35	50.9	9.1	48.0*
R36	50.9	11.8	50.1*
R37	51.9	11.3	49.8*
R38	47.0	5.9	51.3*
R39	50.7	7.2	51.6*
R40	52.1	not located	54.5*
R41	53.7	6.9	49.9*
R42	51.2	13.1	39.3*
R43	51.2	13.6	50.4*
R44	51.7	18.0	48.0*
R45	49.5	10.9	41.2*
R46	48.0	10.4	46.1*
R47	55.5	not located	66.4
R48	53.1	not located	76.9
R49	52.4	not located	64.5
R50	45.7	7.5	48.8*
R51	43.4	9.2	54.5
R52	36.1	5.0	46.6
R53	46.5	8.4	47.0
R54	45.7	10.9	49.1*
R55	45.1	11.9	51.5
R56	45.1	9.9	46.7*
R57	47.1	9.2	46.0*
R58	45.9	9.0	46.7*
R59	46.2	7.5	50.1*
R60	46.2	9.6	46.2*
R61	47.4	9.0	51.4
R62	47.2	8.7	47.2*
R63	45.8	8.9	46.9*
R64	46.3	12.3	46.1*
R65	46.4	12.2	46.7*
R66	45.9	7.3	50.1
R67	50.5	not located	62.6
R68	46.3	9.2	46.8*
R69	49.6	10.5	48.3*
R70	44.2	9.1	43.9*
R71	45.9	12.8	41.4*
R72	44.4	9.9	40.7*
R73	44.4	3.1	44.7*

R74	42.8	8.1	47.2*
R75	43.1	8.8	47.3
R76	42.8	8.7	45.0*
R77	46.9	13.4	56.0
R78	48.0	17.2	43.3*
R79	51.1	14.9	46.6*
R80	50.7	15.3	50.4*
R81	49.4	11.6	52.1
R82	43.8	9.9	48.6
R83	53.2	18.3	45.7*
R84	51.4	14.7	43.2*
R85	48.8	13.8	48.3
R86	44.4	not located	52.7
R87	41.3	7.3	46.4*
R88	40.9	12.0	33.7*
R89	42.1	10.5	46.8*
R90	42.1	14.8	43.5*
R91	37.9	8.8	35.8*
R92	34.4	8.7	32.4*
R93	28.6	3.8	26.6*
R94	42.8	not located	73.4
R95	46.6	not located	63.9
R96	49.6	not located	65.8
R97	35.3	8.0	47.5
R98	18.3	0.7	34.1
R99	33.3	7.5	48.9
R100	10.5	–9.6	31.2
R101	42.9	7.9	47.3
R102	41.1	9.9	39.0
R103	40.6	9.7	46.0
R104	41.8	9.2	44.0
R105	41.9	7.6	43.3
R106	41.9	9.5	43.7
R107	36.3	11.4	40.2*
R108	43.0	7.7	56.3
R109	39.1	10.5	50.2
R110	41.7	12.6	53.2
R111	39.3	8.9	43.7
R112	42.0	8.9	44.2

R113	40.5	8.9	44.6
R114	41.1	11.1	44.5*
R115	39.5	12.1	45.9*
R116	32.9	5.2	47.6
R117	37.9	7.3	50.3
R118	35.1	9.1	46.9
R119	38.7	12.2	39.5*
R120	38.6	15.3	35.6*
R121	36.7	11.5	39.2
R122	33.3	9.2	40.0
R123	37.1	8.1	37.1*
R124	37.1	11.3	32.9*
R125	37.3	8.4	46.4
R126	46.9	14.6	42.2*

Supplementary Table 5: Physicochemical properties of radicals. E_{SOMO}, the energy of SOMO, values in kcal/mol. **BV(r=3),** the buried volume within a 3 Å radius of the bond formation carbon center, values in %.

Radicals	E_{SOMO}	$BV(r=3)$
R1	–106.3	64.2
R2	–119.9	57.5
R3	–111.8	61.3
R4	–104.5	68.7
R5	–112.3	49.2
R6	–102.0	77.5
R7	–126.9	64.3
R8	–121.8	64.0
R9	–86.8	64.2
R10	–101.9	63.5
R11	–142.9	61.4
R12	–132.1	75.4
R13	–121.5	77.8
R14	–140.7	26.7
R15	–140.3	49.9
R16	–159.9	45.8
R17	–146.1	46.0
R18	–136.1	51.2
R19	–164.6	41.3

R20	–83.4	49.3
R21	–104.7	56.4
R22	–107.2	69.0
R23	–108.3	49.1
R24	–118.6	51.8
R25	–120.7	49.2
R26	–116.7	49.2
R27	–112.4	49.2
R28	–118.3	49.2
R29	–133.8	49.2
R30	–90.0	49.1
R31	–110.2	49.2
R32	–108.4	52.1
R33	–121.9	47.9
R34	–120.7	49.0
R35	–129.6	48.9
R36	–120.7	48.0
R37	–119.0	50.7
R38	–108.1	48.4
R39	–110.3	48.1
R40	–111.6	59.2
R41	–126.3	65.7
R42	–141.6	61.6
R43	–133.3	65.8
R44	–131.4	66.3
R45	–148.9	57.1
R46	–145.4	69.7
R47	–97.5	58.9
R48	–78.3	64.3
R49	–91.6	65.1
R50	–106.2	75.5
R51	–98.3	69.5
R52	–111.0	84.1
R53	–102.9	64.2
R54	–104.4	64.3
R55	–104.7	66.9
R56	–112.7	66.7
R57	–114.4	64.2

R58	–111.0	64.2
R59	–106.8	64.2
R60	–112.5	64.3
R61	–96.1	65.3
R62	–113.1	63.2
R63	–114.1	64.1
R64	–114.0	63.1
R65	–112.7	65.8
R66	–105.2	63.4
R67	–104.3	70.9
R68	–115.5	70.6
R69	–112.7	66.6
R70	–125.3	65.9
R71	–127.7	66.1
R72	–132.2	62.0
R73	–122.3	64.1
R74	–108.2	57.6
R75	–108.2	61.8
R76	–113.3	57.6
R77	–97.0	70.0
R78	–121.3	70.7
R79	–116.4	77.1
R80	–106.6	72.8
R81	–108.1	69.2
R82	–104.5	45.8
R83	–129.8	79.0
R84	–126.3	76.1
R85	–111.8	66.8
R86	–104.1	73.8
R87	–117.9	79.5
R88	–134.6	75.5
R89	–123.6	79.2
R90	–124.8	79.7
R91	–137.9	71.8
R92	–134.9	82.6
R93	–133.4	90.3
R94	–75.0	77.5
R95	–98.5	79.1

R96	–92.1	72.7
R97	–101.8	86.5
R98	–109.4	96.0
R99	–101.2	84.4
R100	–108.2	94.8
R101	–99.0	77.5
R102	–106.8	79.1
R103	–109.5	77.5
R104	–106.7	77.5
R105	–102.7	77.5
R106	–108.1	77.5
R107	–121.7	77.6
R108	–84.8	77.5
R109	–101.4	77.5
R110	–99.7	79.3
R111	–107.9	76.7
R112	–109.0	77.4
R113	–115.9	77.4
R114	–108.2	76.8
R115	–107.8	78.1
R116	–97.7	76.9
R117	–99.1	76.9
R118	–111.3	82.8
R119	–124.2	77.9
R120	–130.8	83.0
R121	–114.3	84.5
R122	–120.6	89.9
R123	–126.9	75.5
R124	–134.5	80.9
R125	–101.1	80.9
R126	–138.1	68.1

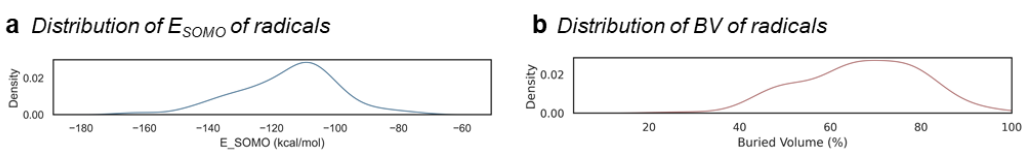

Supplementary Figure 7: Physicochemical property distribution of radicals.

2.3 Nucleophiles.

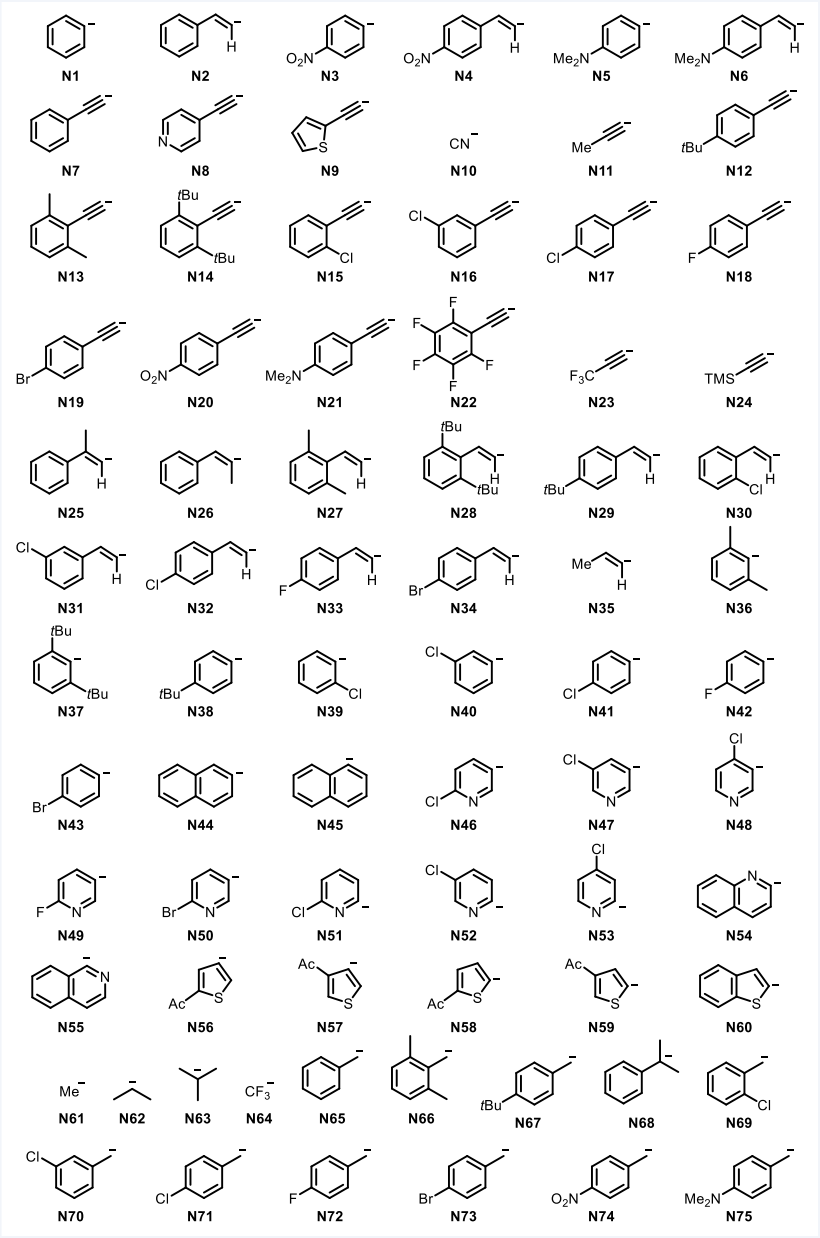

Supplementary Figure 8: Numbering of nucleophiles involved in this study.

Supplementary Table 6: LFER parameters of nucleophiles for RE, RS and IP processes. *, the corresponding radical substitution transition states for these nucleophiles not located. However, N_{RS} values of these radicals can be derived using linear transformation from N_{RE} values, as shown in Section 5.3 and Supplementary Figure 17.

Nucleophiles	N_{RE}	N_{RS}	N_{IP}
N1	20.6	92.3	27.0
N2	18.9	88.8	26.1

N3	2.5	76.8*	12.5
N4	2.8	74.8	11.6
N5	23.9	95.3	28.5
N6	23.3	91.1	26.4
N7	–3.9	73.9	17.4
N8	–11.7	67.1	9.0
N9	–6.9	71.0	16.7
N10	–17.4	62.3	5.1
N11	8.9	82.9	26.1
N12	–3.4	74.5	13.8
N13	–3.5	72.9	not located
N14	–5.7	69.6	12.8
N15	–7.0	69.3	16.4
N16	–9.5	68.8	not located
N17	–8.3	70.3	14.2
N18	–6.2	72.0	16.1
N19	–8.9	69.6	8.8
N20	–19.6	60.1	3.1
N21	0.3	77.1	21.2
N22	–17.8	62.2	4.4
N23	–20.0	60.7	2.5
N24	–2.8	74.7	16.1
N25	20.5	88.9	26.0
N26	22.9	89.0	23.0
N27	19.0	88.7*	21.7
N28	17.6	82.4	14.8
N29	19.8	90.2	25.1
N30	16.9	88.1	22.1
N31	12.8	84.4	19.9
N32	14.7	85.5	20.9
N33	16.7	85.4	22.2
N34	14.8	84.6	19.7
N35	29.1	97.2	31.1
N36	15.6	86.3*	not located
N37	–7.8	69.4*	not located
N38	21.3	90.4*	26.6
N39	3.9	77.9*	14.2
N40	10.5	82.6*	18.8
N41	12.9	84.3*	21.6

N42	14.9	85.8*	22.6
N43	11.3	83.2*	20.1
N44	14.0	84.0	23.4
N45	13.9	85.0*	19.0
N46	1.9	74.2	12.0
N47	5.6	80.1	19.3
N48	–0.6	73.9	10.6
N49	2.8	75.0	12.5
N50	–1.3	71.2	8.9
N51	14.3	88.0	23.5
N52	16.7	89.9	23.7
N53	15.2	85.8	21.9
N54	22.0	90.9*	26.7
N55	19.3	89.0*	24.4
N56	5.1	78.4	12.0
N57	3.6	77.6*	16.2
N58	–4.5	70.7	8.4
N59	1.6	75.7	12.7
N60	3.0	76.3	15.3
N61	28.6	not located	31.4
N62	28.1	not located	20.6
N63	12.7	not located	–0.4
N64	–24.3	not located	–2.8
N65	0.1	not located	–1.0
N66	–11.7	not located	–16.2
N67	3.2	not located	–0.7
N68	–6.8	not located	–5.3
N69	–9.6	not located	–10.3
N70	–5.7	not located	–8.1
N71	–3.2	not located	–6.4
N72	1.3	not located	–1.9
N73	–6.3	not located	–8.9
N74	–31.9	not located	–29.1
N75	4.5	not located	1.1

Supplementary Table 7: Physicochemical properties of nucleophiles. E_{HOMO}, the energy of HOMO, values in kcal/mol. **BV(r=3),** the buried volume within a 3 Å radius of the bond formation carbon center, values in %.

Nucleophiles	E_{HOMO}	$BV(r=3)$

N1	37.9	52.6
N2	26.5	40.1
N3	10.0	52.6
N4	0.2	40.1
N5	34.0	52.5
N6	26.1	40.1
N7	–7.0	30.2
N8	–19.5	30.2
N9	–6.5	29.9
N10	12.5	22.1
N11	19.5	29.3
N12	–8.9	30.2
N13	–9.9	35.2
N14	–20.4	47.2
N15	–15.0	31.7
N16	–16.7	30.3
N17	–15.2	30.2
N18	–8.7	30.2
N19	–17.1	30.2
N20	–36.0	30.3
N21	–6.0	30.3
N22	–24.1	31.4
N23	–16.8	30.0
N24	–9.0	30.8
N25	24.2	44.9
N26	32.6	54.7
N27	26.9	44.5
N28	17.4	55.1
N29	24.5	40.1
N30	19.9	40.5
N31	18.1	40.2
N32	19.0	40.2
N33	24.4	40.2
N34	17.2	40.2
N35	52.9	38.3
N36	31.9	60.9
N37	15.1	78.8
N38	32.8	52.4

N39	7.6	56.1
N40	20.9	53.0
N41	25.6	52.6
N42	32.4	52.6
N43	22.0	52.6
N44	24.5	52.6
N45	22.8	56.3
N46	15.8	52.2
N47	14.7	52.6
N48	1.4	55.6
N49	24.1	52.2
N50	7.9	52.3
N51	20.7	49.4
N52	28.8	49.5
N53	23.7	50.0
N54	31.0	49.5
N55	28.5	53.2
N56	6.8	51.6
N57	8.6	56.1
N58	–8.5	51.3
N59	–1.3	50.9
N60	–2.6	51.2
N61	86.7	25.6
N62	72.9	57.0
N63	64.4	71.2
N64	34.0	47.2
N65	40.1	48.9
N66	37.2	77.4
N67	34.6	48.9
N68	33.8	56.6
N69	28.5	51.6
N70	27.6	49.0
N71	29.5	49.0
N72	38.8	48.9
N73	26.8	49.0
N74	–0.8	49.2
N75	34.7	48.9

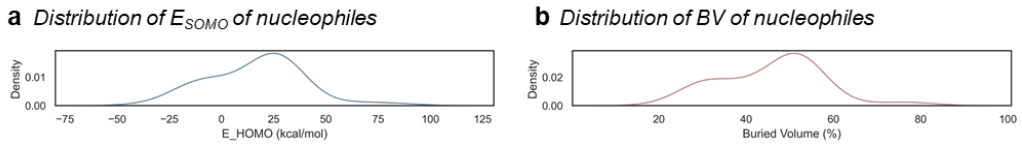

Supplementary Figure 9: Physicochemical property distribution of nucleophiles.

3 Validation of the LFER Model.

We examined the LFER approach in terms of four key aspects: DFT reliability, the impact of density functionals, solvent effects, and the cross-validation on the LFER methodology. These results collectively support the reliability of the LFER model developed in this work.

3.1 DFT Calculation Reliability.

To assess the accuracy of our computational protocol, we benchmarked the DFT method employed in this study against the high-level DLPNO-CCSD(T) approach, which is widely regarded as the gold standard for reaction energetics. For two representative radical bond formation reactions involving distinctive ligands, radicals and nucleophiles, we calculated the free energy differences between the reductive elimination (RE) and ion-pair-type (IP) pathways and directly compared the DFT results with those from DLPNO-CCSD(T) (Supplementary Figure 10). The two levels of theory show excellent agreement, with deviations of only 1.6 kcal/mol and 0.8 kcal/mol, respectively. This close correspondence strongly supports the reliability of our chosen DFT protocol for capturing the mechanistic selectivity in these copper-catalyzed radical bond formation reactions.

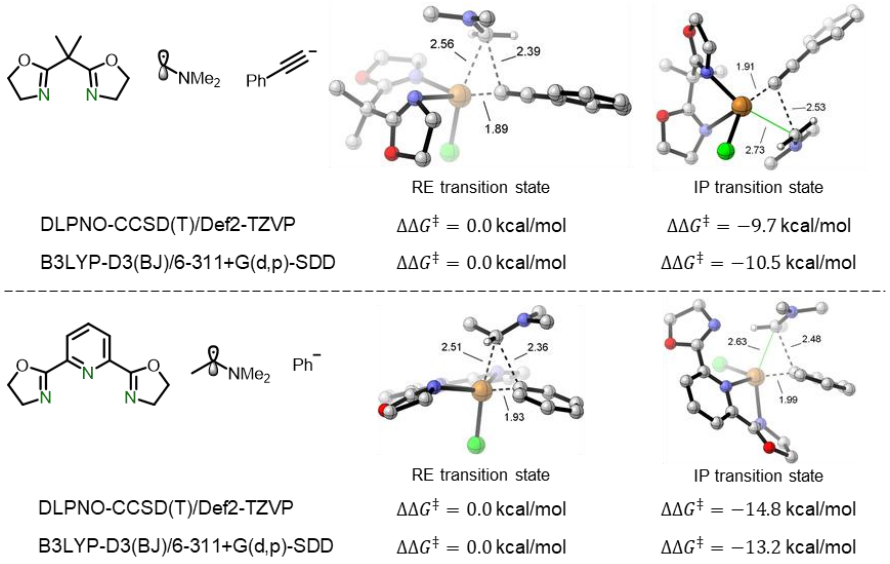

Supplementary Figure 10: Benchmarking of DFT against DLPNO-CCSD(T) for representative copper-catalyzed radical bond formation reactions, transition states optimized at the B3LYP-D3(BJ)/6-31G(d)-LANL2DZ level of theory.

3.2 Density Functional Reliability.

With the basis set kept consistent (6-311+G(d, p)-SDD), different density functionals were employed to calculate the single-point energies of optimized structures (obtained under B3LYP-D3(BJ)/6-31G(d)-LANL2DZ level of theory) of the 250 reactions for constructing LFERs.

The favored bond formation mechanisms and the corresponding free energy changes for each combination under different density functionals are summarized in Supplementary Table 8 and Supplementary Table 9. A high consistency was observed in the favored

mechanisms across the tested density functionals, including B3LYP-D3(BJ), M06, PBE0-D3, and ωB97X-D. The complete free energy changes under different density functionals are available at GitHub: https://github.com/XuGuoXiong/LFER-on-Mechanism-Prediction.git. The B3LYP-D3(BJ)/6-311+G(d,p)-SDD//B3LYP-D3(BJ)/6-31G(d)-LANL2DZ level of theory was selected for DFT calculations based on two key considerations: (1) its proven capability in determining the favored bond formation mechanism, and (2) its established reliability in prior computational studies of copper-catalyzed radical transformations[20].

Supplementary Table 8: Favored bond formation mechanisms for ligand-radical-nucleophile combinations under different density functionals.

Ligand	Radical	Nucleophile	The Favored Bond Formation Mechanism			
			B3LYP-D3(BJ)	M06	PBE0-D3	ωB97X-D
L4	R1	N1	RE	RE	RE	RE
L4	R1	N2	RE	RE	RE	RE
L4	R1	N7	RE	RE	RE	RE
L4	R1	N10	RE	RE	RE	RE
L4	R1	N61	RE	RE	RE	RE
L4	R5	N1	RE	RE	RE	RE
L4	R5	N2	RE	RE	RE	RE
L4	R5	N7	RE	RE	RE	RE
L4	R5	N10	RE	RE	RE	RE
L4	R5	N61	RE	RE	RE	RE
L4	R6	N1	RE	RE	RE	RE
L4	R6	N2	RE	RE	RE	RE
L4	R6	N7	RE	RE	RE	RE
L4	R6	N10	IP	IP	RS	IP
L4	R6	N61	RE	RE	RE	RE
L4	R11	N1	RE	RE	RE	RE
L4	R11	N2	RE	RE	RE	RE
L4	R11	N7	RE	RE	RE	RE
L4	R11	N10	RE	RE	RE	RE
L4	R11	N61	RE	RE	RE	RE
L4	R12	N1	RE	RE	RE	RE
L4	R12	N2	RE	RE	RE	RE
L4	R12	N7	RS	RE	RS	RS
L4	R12	N10	RS	RE	RS	RS
L4	R12	N61	RE	RE	RE	RE
L4	R16	N1	RE	RE	RE	RE
L4	R16	N2	RE	RE	RE	RE
L4	R16	N7	RE	RE	RE	RE
L4	R16	N10	RE	RE	RE	RE
L4	R16	N61	RE	RE	RE	RE

L4	**R20**	**N1**	RE	RE	RE	RE
L4	**R20**	**N2**	RE	RE	RE	RE
L4	**R20**	**N7**	IP	IP	IP	IP
L4	**R20**	**N10**	IP	IP	IP	IP
L4	**R20**	**N61**	RE	RE	RE	RE
L4	**R40**	**N1**	RE	RE	RE	RE
L4	**R40**	**N2**	RE	RE	RE	RE
L4	**R40**	**N7**	RE	RE	RE	RE
L4	**R40**	**N10**	RE	RE	RE	RE
L4	**R40**	**N61**	RE	RE	RE	RE
L4	**R48**	**N1**	IP	IP	IP	IP
L4	**R48**	**N2**	RE	RE	RE	RE
L4	**R48**	**N7**	IP	IP	IP	IP
L4	**R48**	**N10**	IP	IP	IP	IP
L4	**R48**	**N61**	RE	RE	RE	RE
L4	**R94**	**N1**	IP	IP	IP	IP
L4	**R94**	**N2**	IP	IP	IP	IP
L4	**R94**	**N7**	IP	IP	IP	IP
L4	**R94**	**N10**	IP	IP	IP	IP
L4	**R94**	**N61**	IP	IP	IP	IP
L6	**R1**	**N1**	RE	RE	RE	RE
L6	**R1**	**N2**	RE	RE	RE	RE
L6	**R1**	**N7**	RE	RE	RE	RE
L6	**R1**	**N10**	RE	RE	RE	RE
L6	**R1**	**N61**	RE	RE	RE	RE
L6	**R5**	**N1**	RE	RE	RE	RE
L6	**R5**	**N2**	RE	RE	RE	RE
L6	**R5**	**N7**	RE	RE	RE	RE
L6	**R5**	**N10**	RE	RE	RE	RE
L6	**R5**	**N61**	RE	RE	RE	RE
L6	**R6**	**N1**	RE	RE	RE	RE
L6	**R6**	**N2**	RE	RE	RE	RE
L6	**R6**	**N7**	RS	RS	RS	RS
L6	**R6**	**N10**	RS	RS	RS	RS
L6	**R6**	**N61**	RE	RE	RE	RE
L6	**R11**	**N1**	RE	RE	RE	RE
L6	**R11**	**N2**	RE	RE	RE	RE
L6	**R11**	**N7**	RE	RE	RE	RE
L6	**R11**	**N10**	RE	RE	RE	RE

L6	**R11**	**N61**	RE	RE	RE	RE
L6	**R12**	**N1**	RE	RE	RE	RE
L6	**R12**	**N2**	RE	RE	RE	RE
L6	**R12**	**N7**	RS	RE	RS	RS
L6	**R12**	**N10**	RS	RS	RS	RS
L6	**R12**	**N61**	RE	RE	RE	RE
L6	**R16**	**N1**	RE	RE	RE	RE
L6	**R16**	**N2**	RE	RE	RE	RE
L6	**R16**	**N7**	RE	RE	RE	RE
L6	**R16**	**N10**	RE	RE	RE	RE
L6	**R16**	**N61**	RE	RE	RE	RE
L6	**R20**	**N1**	RE	RE	RE	RE
L6	**R20**	**N2**	RE	RE	RE	RE
L6	**R20**	**N10**	IP	IP	IP	IP
L6	**R20**	**N61**	RE	RE	RE	RE
L6	**R40**	**N1**	RE	RE	RE	RE
L6	**R40**	**N2**	RE	RE	RE	RE
L6	**R40**	**N7**	RE	RE	RE	RE
L6	**R40**	**N10**	RE	RE	RE	RE
L6	**R40**	**N61**	RE	RE	RE	RE
L6	**R48**	**N1**	IP	IP	IP	IP
L6	**R48**	**N2**	IP	IP	IP	IP
L6	**R48**	**N7**	IP	IP	IP	IP
L6	**R48**	**N10**	IP	IP	IP	IP
L6	**R48**	**N61**	RE	RE	RE	RE
L6	**R94**	**N1**	IP	IP	IP	IP
L6	**R94**	**N2**	IP	IP	IP	IP
L6	**R94**	**N7**	IP	IP	IP	IP
L6	**R94**	**N10**	IP	IP	IP	IP
L6	**R94**	**N61**	IP	IP	IP	IP
L7	**R1**	**N1**	RE	RE	RE	RE
L7	**R1**	**N2**	RE	RE	RE	RE
L7	**R1**	**N7**	RE	RE	RE	RE
L7	**R1**	**N10**	RE	RE	RE	RE
L7	**R1**	**N61**	RE	RE	RE	RE
L7	**R5**	**N1**	RE	RE	RE	RE
L7	**R5**	**N2**	RE	RE	RE	RE
L7	**R5**	**N7**	RE	RE	RE	RE
L7	**R5**	**N10**	RE	RE	RE	RE

L7	**R5**	**N61**	RE	RE	RE	RE
L7	**R6**	**N1**	RE	RE	RE	RE
L7	**R6**	**N2**	RE	RE	RE	RE
L7	**R6**	**N7**	RE	RE	RE	RE
L7	**R6**	**N10**	IP	IP	IP	IP
L7	**R6**	**N61**	RE	RE	RE	RE
L7	**R11**	**N1**	RE	RE	RE	RE
L7	**R11**	**N2**	RE	RE	RE	RE
L7	**R11**	**N7**	RE	RE	RE	RE
L7	**R11**	**N10**	RE	RE	RE	RE
L7	**R11**	**N61**	RE	RE	RE	RE
L7	**R12**	**N1**	RE	RE	RE	RE
L7	**R12**	**N2**	RE	RE	RE	RE
L7	**R12**	**N7**	RE	RE	RE	RE
L7	**R12**	**N10**	RE	RE	RE	RE
L7	**R12**	**N61**	RE	RE	RE	RE
L7	**R16**	**N1**	RE	RE	RE	RE
L7	**R16**	**N2**	RE	RE	RE	RE
L7	**R16**	**N7**	RE	RE	RE	RE
L7	**R16**	**N10**	RE	RE	RE	RE
L7	**R16**	**N61**	RE	RE	RE	RE
L7	**R20**	**N1**	RE	RE	RE	RE
L7	**R20**	**N2**	RE	RE	RE	RE
L7	**R20**	**N7**	IP	IP	IP	IP
L7	**R20**	**N10**	IP	IP	IP	IP
L7	**R20**	**N61**	RE	RE	RE	RE
L7	**R40**	**N1**	RE	RE	RE	RE
L7	**R40**	**N2**	RE	RE	RE	RE
L7	**R40**	**N7**	RE	RE	RE	RE
L7	**R40**	**N10**	RE	RE	RE	RE
L7	**R40**	**N61**	RE	RE	RE	RE
L7	**R48**	**N1**	IP	IP	IP	IP
L7	**R48**	**N2**	IP	IP	IP	IP
L7	**R48**	**N7**	IP	IP	IP	IP
L7	**R48**	**N10**	IP	IP	IP	IP
L7	**R48**	**N61**	RE	RE	RE	RE
L7	**R94**	**N1**	IP	IP	IP	IP
L7	**R94**	**N2**	IP	IP	IP	IP
L7	**R94**	**N7**	IP	IP	IP	IP

L7	**R94**	**N10**	IP	IP	IP	IP
L7	**R94**	**N61**	RE	RE	RE	RE
L10	**R1**	**N1**	RE	RE	RE	RE
L10	**R1**	**N2**	RE	RE	RE	RE
L10	**R1**	**N7**	RE	RE	RE	RE
L10	**R1**	**N10**	RE	RE	RE	RE
L10	**R1**	**N61**	RE	RE	RE	RE
L10	**R5**	**N1**	RE	RE	RE	RE
L10	**R5**	**N2**	RE	RE	RE	RE
L10	**R5**	**N7**	RE	RE	RE	RE
L10	**R5**	**N10**	RE	RE	RE	RE
L10	**R5**	**N61**	RE	RE	RE	RE
L10	**R6**	**N1**	RE	RE	RE	RE
L10	**R6**	**N2**	RE	RE	RE	RE
L10	**R6**	**N7**	RE	RE	RE	RE
L10	**R6**	**N10**	RE	RE	RE	RE
L10	**R6**	**N61**	RE	RE	RE	RE
L10	**R11**	**N1**	RE	RE	RE	RE
L10	**R11**	**N2**	RE	RE	RE	RE
L10	**R11**	**N7**	RE	RE	RE	RE
L10	**R11**	**N10**	RE	RE	RE	RE
L10	**R11**	**N61**	RE	RE	RE	RE
L10	**R12**	**N1**	RE	RE	RE	RE
L10	**R12**	**N2**	RE	RE	RE	RE
L10	**R12**	**N7**	RE	RE	RE	RE
L10	**R12**	**N10**	RE	RE	RE	RE
L10	**R12**	**N61**	RE	RE	RE	RE
L10	**R16**	**N1**	RE	RE	RE	RE
L10	**R16**	**N2**	RE	RE	RE	RE
L10	**R16**	**N7**	RE	RE	RE	RE
L10	**R16**	**N10**	RE	RE	RE	RE
L10	**R16**	**N61**	RE	RE	RE	RE
L10	**R20**	**N1**	RE	RE	RE	RE
L10	**R20**	**N2**	RE	RE	RE	RE
L10	**R20**	**N10**	IP	IP	IP	IP
L10	**R20**	**N61**	RE	RE	RE	RE
L10	**R40**	**N1**	RE	RE	RE	RE
L10	**R40**	**N2**	RE	RE	RE	RE
L10	**R40**	**N7**	RE	RE	RE	RE

L10	**R40**	**N10**	RE	RE	RE	RE
L10	**R40**	**N61**	RE	RE	RE	RE
L10	**R48**	**N1**	IP	IP	IP	IP
L10	**R48**	**N2**	IP	IP	IP	IP
L10	**R48**	**N10**	IP	IP	IP	IP
L10	**R48**	**N61**	RE	RE	RE	RE
L10	**R94**	**N1**	IP	IP	IP	IP
L10	**R94**	**N2**	RE	RE	RE	RE
L10	**R94**	**N7**	IP	IP	IP	IP
L10	**R94**	**N10**	IP	IP	IP	IP
L10	**R94**	**N61**	IP	IP	IP	IP
L14	**R1**	**N1**	RE	RE	RE	RE
L14	**R1**	**N2**	RE	RE	RE	RE
L14	**R1**	**N7**	RS	RE	RS	RS
L14	**R1**	**N10**	RS	RE	RS	RS
L14	**R1**	**N61**	RE	RE	RE	RE
L14	**R5**	**N1**	RE	RE	RE	RE
L14	**R5**	**N2**	RE	RE	RE	RE
L14	**R5**	**N7**	RE	RE	RS	RE
L14	**R5**	**N10**	RE	RE	RE	RE
L14	**R5**	**N61**	RE	RE	RE	RE
L14	**R6**	**N1**	RE	RE	RE	RE
L14	**R6**	**N2**	RE	RE	RE	RE
L14	**R6**	**N7**	RS	RS	RS	RS
L14	**R6**	**N10**	RS	RS	RS	RS
L14	**R6**	**N61**	RE	RE	RE	RE
L14	**R11**	**N1**	RE	RE	RE	RE
L14	**R11**	**N2**	RE	RE	RE	RE
L14	**R11**	**N7**	RS	RE	RS	RS
L14	**R11**	**N10**	RS	RS	RS	RS
L14	**R11**	**N61**	RE	RE	RE	RE
L14	**R12**	**N1**	RE	RE	RE	RE
L14	**R12**	**N2**	RE	RE	RE	RE
L14	**R12**	**N7**	RS	RS	RS	RS
L14	**R12**	**N10**	RS	RS	RS	RS
L14	**R12**	**N61**	RE	RE	RE	RE
L14	**R16**	**N1**	RE	RE	RE	RE
L14	**R16**	**N2**	RE	RE	RE	RE
L14	**R16**	**N7**	RS	RE	RS	RS

L14	**R16**	**N10**	RS	RS	RS	RS
L14	**R16**	**N61**	RE	RE	RE	RE
L14	**R20**	**N1**	RE	RE	RE	RE
L14	**R20**	**N2**	RE	RE	RE	RE
L14	**R20**	**N7**	IP	IP	IP	IP
L14	**R20**	**N10**	IP	IP	IP	IP
L14	**R20**	**N61**	RE	RE	RE	RE
L14	**R40**	**N1**	RE	RE	RE	RE
L14	**R40**	**N2**	RE	RE	RE	RE
L14	**R40**	**N7**	RE	RE	RE	RE
L14	**R40**	**N10**	RE	RE	RE	RE
L14	**R40**	**N61**	RE	RE	RE	RE
L14	**R48**	**N1**	IP	IP	IP	IP
L14	**R48**	**N2**	IP	IP	IP	IP
L14	**R48**	**N7**	IP	IP	IP	IP
L14	**R48**	**N10**	IP	IP	IP	IP
L14	**R48**	**N61**	IP	IP	IP	IP
L14	**R94**	**N1**	IP	IP	IP	IP
L14	**R94**	**N2**	IP	IP	IP	IP
L14	**R94**	**N7**	IP	IP	IP	IP
L14	**R94**	**N10**	IP	IP	IP	IP
L14	**R94**	**N61**	IP	IP	IP	IP

LFER models were established using the free energy changes of bond formation transition states for various combinations under different density functionals, as shown in Fig. 3c, 3d, and 3e in the main text. The fitting results of these LFER models are presented in Supplementary Table 9.

Supplementary Table 9: Performance of LFER model establishment under different density functionals.

Density Functional	Mechanism	R^2	MAE
M06	RE	0.993	1.5
M06	RS	0.972	1.6
M06	IP	0.988	1.4
PBE0-D3	RE	0.994	1.5
PBE0-D3	RS	0.978	1.5
PBE0-D3	IP	0.989	1.5
ωB97X-D	RE	0.994	1.5
ωB97X-D	RS	0.979	1.6
ωB97X-D	IP	0.989	1.5

3.3 Solvent Effect.

Supplementary Figure 11 presents a subset of the reactions for constructing LFERs (Fig. 3a in the main text) for investigating solvent

effects.

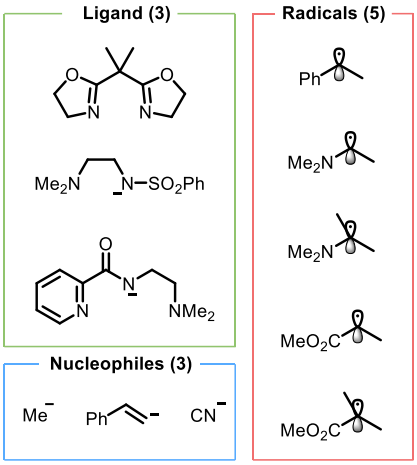

Supplementary Figure 11: A subset for investigating solvent effects.

We investigated the influence of the solvent environment on the construction of the LFER model. A series of common solvents with varying polarities, such as cyclohexane, benzene, THF, DCM, MeCN, and TFEA, were considered. DFT calculations of the combinations within the selected subset on solvent effect were performed under B3LYP-D3(BJ)/6-311+G(d,p)-SDD-SMD(solvent)//B3LYP-D3(BJ)/6-31G(d)-LANL2DZ level of theory.

Supplementary Table 10: Favored bond formation mechanisms for ligand-radical-nucleophile combinations in the gas phase and various solvents.

Results for ligand-radical-nucleophile combinations with only one identifiable bond formation mechanism are omitted to facilitate a more effective comparison across different solvents.

Ligand	Radical	Nucleophile	The Favored Bond Formation Mechanism						
			Gas	Cyclohexane	Benzene	THF	DCM	MeCN	TFEA
L14	**R1**	**N10**	RS	RS	RS	RS	RS	RS	RS
L14	**R11**	**N10**	RS	RS	RS	RS	RS	RS	RS
L14	**R11**	**N2**	RE	RE	RE	RE	RE	RE	RE
L4	**R1**	**N10**	RE	RE	RE	RE	RE	RE	RS
L4	**R6**	**N10**	IP	IP	IP	RS	RS	RS	RS
L4	**R6**	**N2**	RE	RE	RE	RE	RE	RE	RE
L4	**R94**	**N61**	IP	IP	IP	IP	IP	IP	IP
L7	**R11**	**N10**	RE	RE	RE	RE	RE	RE	RE
L7	**R11**	**N2**	RE	RE	RE	RE	RE	RE	RE

Supplementary Table 11: Free energy changes of different ligand-radical-nucleophile combinations in three bond formation processes in different solvents.

The favored bond formation mechanisms and the corresponding free energy changes for each combination in different solvents are summarized. We observed that the favored bond formation mechanism of different ligand-radical-nucleophile combinations in nonpolar and low-polarity solvents (e.g., cyclohexane, benzene, THF, DCM) is highly consistent with that in the gas phase, with only one combination exhibiting competitive mechanisms and showing a different favored mechanism in low-polarity solvents (see Entries 15-17). In contrast, in high-polarity solvents (e.g., MeCN and TFEA), two combinations displayed different favored mechanisms compared to the

gas phase results (see Entries 11-12 and 15-17). These results suggest that the LFER model and parameters obtained in the gas phase are well-suited for predicting bond formation mechanism selectivity in nonpolar and low-polar solvents without additional adjustments. However, accurate predictions in high-polarity solvents require consideration of solvation corrections. Data for ligand-radical-nucleophile combinations with only one identifiable bond formation mechanism are omitted for clarity. The complete free energy changes in different solvents are available at GitHub: https://github.com/XuGuoXiong/LFER-on-Mechanism-Prediction.git.

Entry	Ligand	Radical	Nucleophile	Mechanism	Free Energy Changes (kcal/mol)						
					Gas	Benzene	Cyclohexane	DCM	MeCN	TFEA	THF
1	**L7**	**R11**	**N10**	RE	–139.6	–76.4	–83.2	–35.3	–25.1	–28.2	–39.4
2	**L7**	**R11**	**N10**	RS	–133.0	–69.0	–76.0	–26.4	–15.2	–19.7	–30.6
3	**L7**	**R11**	**N2**	RE	–180.0	–122.2	–128.7	–80.9	–70.3	–73.0	–85.7
4	**L7**	**R11**	**N2**	RS	–163.0	–103.4	–110.3	–59.3	–46.7	–50.3	–63.9
5	**L14**	**R11**	**N10**	RE	–118.6	–53.1	–60.2	–9.9	2.3	–3.8	–13.2
6	**L14**	**R11**	**N10**	RS	–125.8	–60.7	–67.8	–17.7	–5.8	–12.9	–21.2
7	**L14**	**R11**	**N2**	RE	–156.7	–95.2	–102.2	–51.6	–39.2	–44.6	–55.1
8	**L14**	**R11**	**N2**	RS	–150.6	–89.2	–96.2	–45.5	–32.7	–39.2	–49.3
9	**L14**	**R1**	**N10**	RE	–119.0	–53.2	–60.3	–9.6	2.3	–2.8	–13.4
10	**L14**	**R1**	**N10**	RS	–122.2	–57.3	–64.2	–15.5	–4.6	–10.4	–19.5
11	**L4**	**R1**	**N10**	RE	–111.9	–49.5	–56.1	–11.6	–3.5	–6.5	–15.2
12	**L4**	**R1**	**N10**	RS	–106.6	–48.1	–54.5	–11.2	–3.2	–6.9	–14.8
13	**L4**	**R94**	**N61**	IP	–157.1	–93.1	–100.2	–51.4	–41.7	–44.1	–55.3
14	**L4**	**R94**	**N61**	RE	–143.9	–79.8	–86.9	–37.6	–27.1	–28.8	–41.8
15	**L4**	**R6**	**N10**	IP	–107.8	–46.9	–53.3	–10.2	–1.7	–5.6	–13.8
16	**L4**	**R6**	**N10**	RE	–100.9	–39.4	–45.9	–3.6	4.5	1.4	–7.2
17	**L4**	**R6**	**N10**	RS	–106.5	–46.2	–52.5	–10.7	–2.7	–6.5	–14.4
18	**L4**	**R6**	**N2**	RE	–138.5	–80.9	–87.2	–42.9	–33.6	–36.4	–47.2
19	**L4**	**R6**	**N2**	RS	–134.6	–75.8	–82.2	–36.6	–26.7	–29.3	–41.0

LFER models were established using the free energy changes of bond formation transition states for various combinations in different solvents. The fitting results of these LFER models are presented in Supplementary Table 12.

Supplementary Table 12: Performance of LFER model establishment in different solvents.

Solvent	Mechanism	R^2
Benzene	RE	0.992
Benzene	RS	0.997
Benzene	IP	0.995
Cyclohexane	RE	0.992
Cyclohexane	RS	0.997
Cyclohexane	IP	0.995
DCM	RE	0.988
DCM	RS	0.994
DCM	IP	0.995

MeCN	RE	0.987
MeCN	RS	0.992
MeCN	IP	0.995
TFEA	RE	0.984
TFEA	RS	0.991
TFEA	IP	0.994
THF	RE	0.989
THF	RS	0.994
THF	IP	0.995

3.4 5-fold Cross Validation.

Because construction of the LFER equation requires a fixed set of reactions as the reference, the validation cannot be carried out through a conventional random split of the full dataset. If certain reference reactions were excluded from the training set, it would not be possible to construct the corresponding LFER parameters, and as a result, predictions for some test cases could not be performed.

Therefore, in the revised manuscript we implemented a validation scheme inspired by k-fold cross-validation, while keeping the reference reactions fixed (Supplementary Figure 12). Specifically, the remaining 232 reactions were randomly divided into five folds. In each iteration, four folds were combined with the reference reactions to construct the LFER model, and the remaining fold (47 reactions) was used for validation. This strategy preserves the reference requirement intrinsic to the LFER framework, while maintaining the breadth and independence emphasized in k-fold approaches.

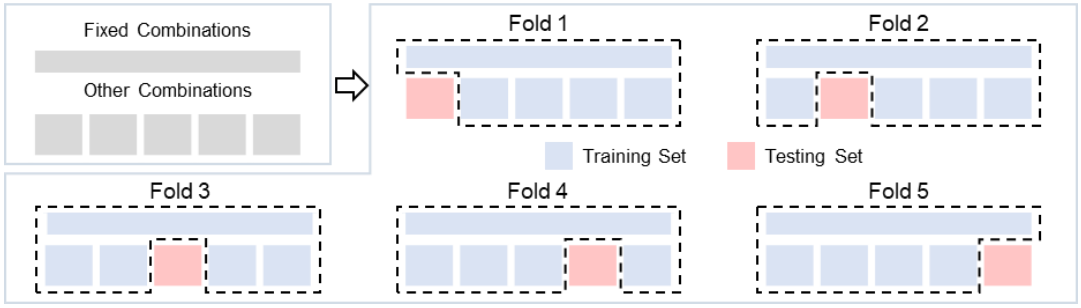

Supplementary Figure 12: Modified 5-fold validation scheme.

Considering the randomness of the 5-fold process, we have conducted 10 repetitions using different random states. Supplementary Table 13 presents a summary of the average results from these 10 trials. The implementation code and detailed data are available on GitHub: https://github.com/XuGuoXiong/LFER-on-Mechanism-Prediction.git.

Supplementary Table 13: Summary validation results for RE, RS, and IP pathways.

Mechanism	R^2 of test set	MAE of test set	RMSE of test Set
RE	0.991 ± 0.001	1.74 ± 0.04	2.18 ± 0.04
RS	0.957 ± 0.012	1.89 ± 0.10	2.56 ± 0.13
IP	0.959 ± 0.014	2.12 ± 0.18	2.67 ± 0.19

4 Reactions for Constructing and Testing LFERs.

This section is divided into four parts: 4.1, Data splitting criteria for select reactions for constructing and testing LFERs; 4.2, Free

energy changes for bond formation processes of reactions for constructing LFERs in Fig. 3a of the main text; 4.3, Another efficient method for generating LFER parameters of components in transformations beyond the 250 reactions for constructing LFERs in Fig. 3a of the main text; and 4.4, Free energy changes for bond formation processes of reactions for testing LFERs in Fig. 3a of the main text.

4.1 Data Splitting Criteria.

For the reactions for constructing LFERs, since the construction of the LFER model requires fitting over a complete set of three-component combinations of ligands, radicals, and nucleophiles to systematically evaluate the feasibility of linear correlations, it was necessary to restrict the number of ligands, radicals, and nucleophiles included. Specifically, we selected 5 ligands, 10 radicals, and 5 nucleophiles (Fig. 3a in the main text). Following the same rationale used in constructing the broader chemical space, we ensured that the reactions for constructing LFERs captured key variations along relevant chemical dimensions: the ligands covered differences in denticity and charge state; the radicals included primary, secondary, and tertiary classes as well as diverse electronic and steric substituent effects; and the nucleophiles represented *sp*, sp^2, and sp^3 hybridization types. These species combined to form 250 reactions, corresponding to 750 possible bond formation transition states. We computed the associated activation barriers and used them to construct the reactions for constructing LFERs for the LFER model (Supplementary Table 14 to Supplementary Table 16 in section 4.2 below).

For the reactions for testing LFERs, our goal was to rigorously challenge the extrapolative power and reliability of the model. To this end, we intentionally avoided reusing molecular structures already present in the reactions for constructing LFERs. Considering the combinatorial explosion of possible species, we did not attempt exhaustive enumeration; instead, we designed the test set to maximize chemical diversity by varying ligands, radicals, and nucleophiles simultaneously within each reaction. The test set comprised 67 entirely new reactions (Supplementary Table 18 to Supplementary Table 20 in section 4.4 below). The test set is structurally and physicochemically distinct from the reactions for constructing LFERs, while also improving its coverage across the full energetic range, thereby providing a stringent and balanced evaluation of the model's predictive performance.

To further illustrate the representativeness of the reactions for constructing and testing LFERs, we employed UMAP dimensionality reduction to visualize and compare their distributions with those of the complete set of 132,000 predicted reactions. Based on six key physical-organic descriptors (including the SOMO energy of radicals, the buried volume of radicals, the HOMO energy of nucleophiles, the buried volume of nucleophiles, the SOMO energy of the LCu(II) active catalyst, and the buried volume of the LCu(II) active catalyst), Supplementary Figure 13a shows that the reactions for constructing LFERs (blue) and the reactions for testing LFERs (red) are evenly distributed across the overall chemical space and together span the major regions of interest. In addition, we performed structural visualization using Morgan fingerprints (Supplementary Figure 13b), which again confirmed that the reactions for constructing and testing LFERs are well balanced in structural diversity.

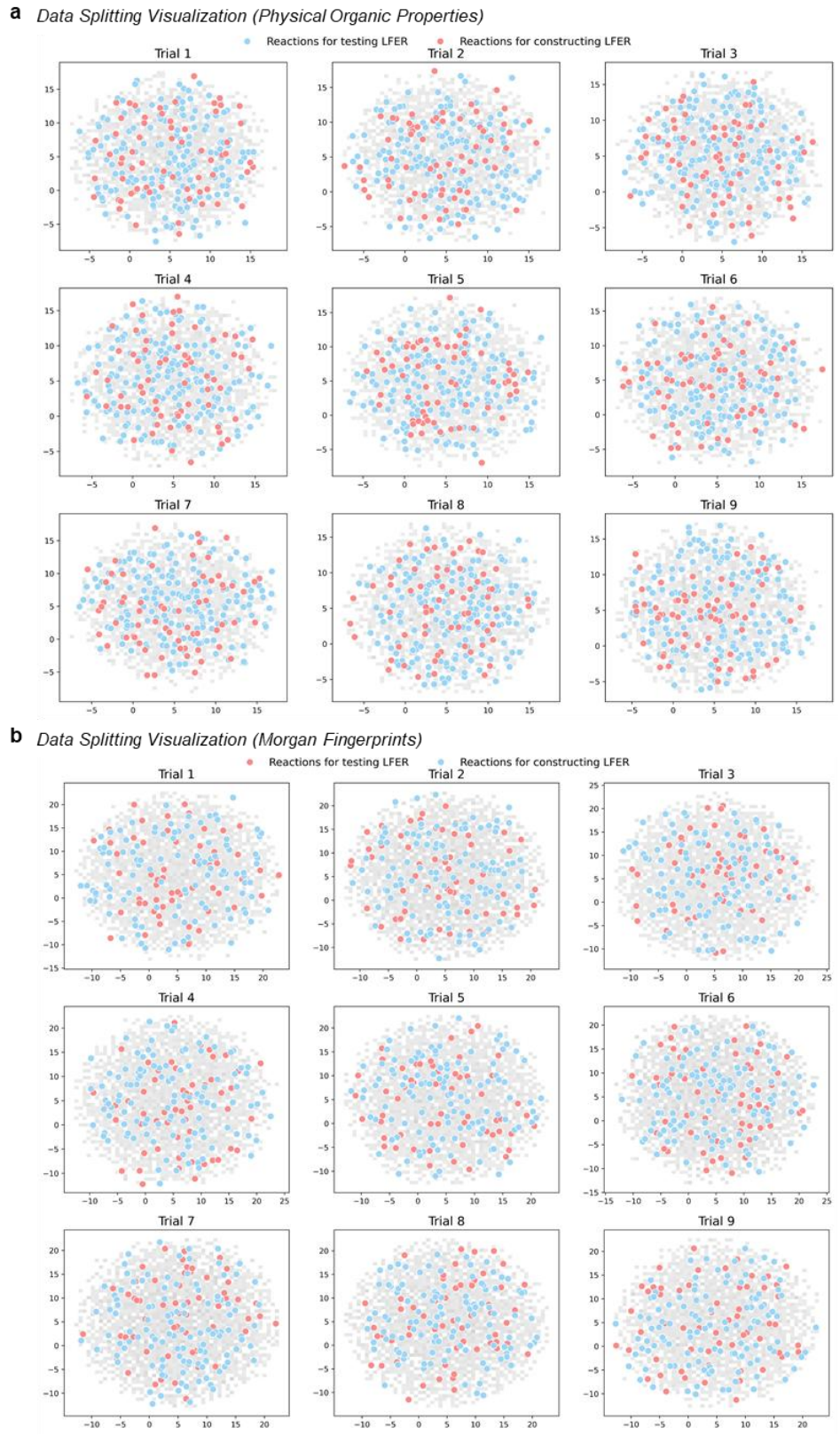

Supplementary Figure 13: UMAP dimensionality reduction visualization. **a** Visualization by physical organic properties. **b** Visualization by Morgan fingerprints.

4.2 Reactions for Constructing LFER.

Supplementary Table 14 to Supplementary Table 16 present the free energy changes of reductive elimination (RE), radical substitution (RS), and ion pair-type bond formation (IP) processes for reactions for constructing LFERs in Fig. 3a of the main text. Quantitative scales of these ligands, radicals and nucleophiles were constructed by subjecting these computed free energy changes to a least-square minimization based on the equation of $\Delta G^{\ddagger} = L + R + N$. Each table includes the following columns: ligand numbering, radical numbering, nucleophile numbering, LFER parameters for the ligand, LFER parameters for the radical, LFER parameters for the nucleophile, free energy changes of bond formation processes obtained from DFT calculations, and free energy changes predicted by the LFER model. According to our LFER model, the free energy changes of bond formation processes can be predicted by simply summing the LFER parameters of the ligand, radical, and nucleophile for the corresponding mechanism.

Supplementary Table 14: Free energy changes for reductive elimination transition states (RE-TS) of reactions for constructing LFERs in Fig. 3a of the main text. a, free energy changes of RE-TS obtained from DFT calculations. **b,** free energy changes of RE-TS predicted by the LFER model in Fig. 3c of the main text.

Ligands	Radicals	Nucleophiles	L_{RE}	R_{RE}	N_{RE}	$\Delta G^{\ddagger}_{RE}$(calc.)[a] (kcal/mol)	$\Delta G^{\ddagger}_{RE}$(pred.)[b] (kcal/mol)
L6	**R16**	**N10**	83.7	54.0	–17.4	–117.0	–120.3
L6	**R20**	**N10**	83.7	55.9	–17.4	not located	–122.2
L6	**R5**	**N10**	83.7	50.4	–17.4	–117.4	–116.7
L6	**R11**	**N10**	83.7	48.5	–17.4	–114.2	–114.8
L6	**R40**	**N10**	83.7	52.1	–17.4	–121.1	–118.4
L6	**R48**	**N10**	83.7	53.1	–17.4	not located	–119.4
L6	**R1**	**N10**	83.7	46.4	–17.4	–114.9	–112.7
L6	**R12**	**N10**	83.7	41.1	–17.4	–107.0	–107.4
L6	**R95**	**N10**	83.7	42.8	–17.4	not located	–109.1
L6	**R6**	**N10**	83.7	39.5	–17.4	–109.6	–105.8
L7	**R16**	**N10**	112.3	54.0	–17.4	–143.2	–148.9
L7	**R20**	**N10**	112.3	55.9	–17.4	not located	–150.8
L7	**R5**	**N10**	112.3	50.4	–17.4	–143.8	–145.3
L7	**R11**	**N10**	112.3	48.5	–17.4	–139.6	–143.4
L7	**R40**	**N10**	112.3	52.1	–17.4	–148.2	–147.0
L7	**R48**	**N10**	112.3	53.1	–17.4	not located	–148.0
L7	**R1**	**N10**	112.3	46.4	–17.4	–141.7	–141.3
L7	**R12**	**N10**	112.3	41.1	–17.4	–134.3	–136.0
L7	**R95**	**N10**	112.3	42.8	–17.4	not located	–137.7
L7	**R6**	**N10**	112.3	39.5	–17.4	not located	–134.4
L14	**R16**	**N10**	88.4	54.0	–17.4	–123.6	–125.0
L14	**R20**	**N10**	88.4	55.9	–17.4	not located	–126.9
L14	**R5**	**N10**	88.4	50.4	–17.4	–121.9	–121.4
L14	**R11**	**N10**	88.4	48.5	–17.4	–118.6	–119.5
L14	**R40**	**N10**	88.4	52.1	–17.4	–124.8	–123.1

L14	**R48**	**N10**	88.4	53.1	–17.4	not located	–124.1
L14	**R1**	**N10**	88.4	46.4	–17.4	–119.0	–117.4
L14	**R12**	**N10**	88.4	41.1	–17.4	not located	–112.1
L14	**R95**	**N10**	88.4	42.8	–17.4	not located	–113.8
L14	**R6**	**N10**	88.4	39.5	–17.4	not located	–110.5
L10	**R16**	**N10**	67.0	54.0	–17.4	–101.9	–103.6
L10	**R20**	**N10**	67.0	55.9	–17.4	not located	–105.5
L10	**R5**	**N10**	67.0	50.4	–17.4	–99.5	–100.0
L10	**R11**	**N10**	67.0	48.5	–17.4	–95.7	–98.1
L10	**R40**	**N10**	67.0	52.1	–17.4	–102.7	–101.7
L10	**R48**	**N10**	67.0	53.1	–17.4	not located	–102.7
L10	**R1**	**N10**	67.0	46.4	–17.4	–97.1	–96.0
L10	**R12**	**N10**	67.0	41.1	–17.4	–90.9	–90.7
L10	**R95**	**N10**	67.0	42.8	–17.4	not located	–92.4
L10	**R6**	**N10**	67.0	39.5	–17.4	–92.6	–89.1
L4	**R16**	**N10**	80.0	54.0	–17.4	–114.5	–116.6
L4	**R20**	**N10**	80.0	55.9	–17.4	not located	–118.5
L4	**R5**	**N10**	80.0	50.4	–17.4	–114.2	–113.0
L4	**R11**	**N10**	80.0	48.5	–17.4	–111.2	–111.1
L4	**R40**	**N10**	80.0	52.1	–17.4	–116.5	–114.7
L4	**R48**	**N10**	80.0	53.1	–17.4	not located	–115.7
L4	**R1**	**N10**	80.0	46.4	–17.4	–111.9	–109.0
L4	**R12**	**N10**	80.0	41.1	–17.4	–103.8	–103.7
L4	**R95**	**N10**	80.0	42.8	–17.4	not located	–105.4
L4	**R6**	**N10**	80.0	39.5	–17.4	–100.9	–102.1
L6	**R16**	**N61**	83.7	54.0	28.6	–168.5	–166.3
L6	**R20**	**N61**	83.7	55.9	28.6	–164.9	–168.2
L6	**R5**	**N61**	83.7	50.4	28.6	–161.4	–162.7
L6	**R11**	**N61**	83.7	48.5	28.6	–162.6	–160.8
L6	**R40**	**N61**	83.7	52.1	28.6	–164.8	–164.4
L6	**R48**	**N61**	83.7	53.1	28.6	–164.5	–165.4
L6	**R1**	**N61**	83.7	46.4	28.6	–157.0	–158.7
L6	**R12**	**N61**	83.7	41.1	28.6	–154.0	–153.4
L6	**R95**	**N61**	83.7	42.8	28.6	not located	–155.1
L6	**R6**	**N61**	83.7	39.5	28.6	–151.5	–151.8
L7	**R16**	**N61**	112.3	54.0	28.6	–192.0	–194.9
L7	**R20**	**N61**	112.3	55.9	28.6	–200.5	–196.8
L7	**R5**	**N61**	112.3	50.4	28.6	–188.5	–191.3
L7	**R11**	**N61**	112.3	48.5	28.6	–187.0	–189.4

L7	**R40**	**N61**	112.3	52.1	28.6	–190.7	–193.0
L7	**R48**	**N61**	112.3	53.1	28.6	–193.7	–194.0
L7	**R1**	**N61**	112.3	46.4	28.6	–184.3	–187.3
L7	**R12**	**N61**	112.3	41.1	28.6	–181.8	–182.0
L7	**R95**	**N61**	112.3	42.8	28.6	–188.4	–183.7
L7	**R6**	**N61**	112.3	39.5	28.6	–180.2	–180.4
L14	**R16**	**N61**	88.4	54.0	28.6	–172.1	–171.0
L14	**R20**	**N61**	88.4	55.9	28.6	–170.6	–172.9
L14	**R5**	**N61**	88.4	50.4	28.6	–166.7	–167.4
L14	**R11**	**N61**	88.4	48.5	28.6	–164.8	–165.5
L14	**R40**	**N61**	88.4	52.1	28.6	–168.9	–169.1
L14	**R48**	**N61**	88.4	53.1	28.6	not located	–170.1
L14	**R1**	**N61**	88.4	46.4	28.6	–162.4	–163.4
L14	**R12**	**N61**	88.4	41.1	28.6	–159.5	–158.1
L14	**R95**	**N61**	88.4	42.8	28.6	not located	–159.8
L14	**R6**	**N61**	88.4	39.5	28.6	–155.3	–156.5
L10	**R16**	**N61**	67.0	54.0	28.6	–155.3	–149.6
L10	**R20**	**N61**	67.0	55.9	28.6	–150.3	–151.5
L10	**R5**	**N61**	67.0	50.4	28.6	–148.5	–146.0
L10	**R11**	**N61**	67.0	48.5	28.6	–148.3	–144.1
L10	**R40**	**N61**	67.0	52.1	28.6	–151.3	–147.7
L10	**R48**	**N61**	67.0	53.1	28.6	–152.0	–148.7
L10	**R1**	**N61**	67.0	46.4	28.6	–144.3	–142.0
L10	**R12**	**N61**	67.0	41.1	28.6	–137.7	–136.7
L10	**R95**	**N61**	67.0	42.8	28.6	not located	–138.4
L10	**R6**	**N61**	67.0	39.5	28.6	–134.2	–135.1
L4	**R16**	**N61**	80.0	54.0	28.6	–165.3	–162.6
L4	**R20**	**N61**	80.0	55.9	28.6	–162.5	–164.5
L4	**R5**	**N61**	80.0	50.4	28.6	–158.3	–159.0
L4	**R11**	**N61**	80.0	48.5	28.6	–157.6	–157.1
L4	**R40**	**N61**	80.0	52.1	28.6	–160.4	–160.7
L4	**R48**	**N61**	80.0	53.1	28.6	–164.2	–161.7
L4	**R1**	**N61**	80.0	46.4	28.6	–152.6	–155.0
L4	**R12**	**N61**	80.0	41.1	28.6	–149.7	–149.7
L4	**R95**	**N61**	80.0	42.8	28.6	–143.9	–151.4
L4	**R6**	**N61**	80.0	39.5	28.6	–146.9	–148.1
L6	**R16**	**N1**	83.7	54.0	20.6	–161.0	–158.3
L6	**R20**	**N1**	83.7	55.9	20.6	–161.4	–160.2
L6	**R5**	**N1**	83.7	50.4	20.6	–156.7	–154.7

L6	**R11**	**N1**	83.7	48.5	20.6	–156.0	–152.8
L6	**R40**	**N1**	83.7	52.1	20.6	–158.4	–156.4
L6	**R48**	**N1**	83.7	53.1	20.6	not located	–157.4
L6	**R1**	**N1**	83.7	46.4	20.6	–148.2	–150.7
L6	**R12**	**N1**	83.7	41.1	20.6	–144.1	–145.4
L6	**R95**	**N1**	83.7	42.8	20.6	not located	–147.1
L6	**R6**	**N1**	83.7	39.5	20.6	–141.2	–143.8
L7	**R16**	**N1**	112.3	54.0	20.6	–189.1	–186.9
L7	**R20**	**N1**	112.3	55.9	20.6	–189.9	–188.8
L7	**R5**	**N1**	112.3	50.4	20.6	–183.8	–183.3
L7	**R11**	**N1**	112.3	48.5	20.6	–181.7	–181.4
L7	**R40**	**N1**	112.3	52.1	20.6	–184.6	–185.0
L7	**R48**	**N1**	112.3	53.1	20.6	not located	–186.0
L7	**R1**	**N1**	112.3	46.4	20.6	–180.1	–179.3
L7	**R12**	**N1**	112.3	41.1	20.6	–173.7	–174.0
L7	**R95**	**N1**	112.3	42.8	20.6	not located	–175.7
L7	**R6**	**N1**	112.3	39.5	20.6	–173.1	–172.4
L14	**R16**	**N1**	88.4	54.0	20.6	–163.5	–163.0
L14	**R20**	**N1**	88.4	55.9	20.6	–163.0	–164.9
L14	**R5**	**N1**	88.4	50.4	20.6	–160.0	–159.4
L14	**R11**	**N1**	88.4	48.5	20.6	–157.0	–157.5
L14	**R40**	**N1**	88.4	52.1	20.6	–159.5	–161.1
L14	**R48**	**N1**	88.4	53.1	20.6	not located	–162.1
L14	**R1**	**N1**	88.4	46.4	20.6	–154.5	–155.4
L14	**R12**	**N1**	88.4	41.1	20.6	–150.2	–150.1
L14	**R95**	**N1**	88.4	42.8	20.6	not located	–151.8
L14	**R6**	**N1**	88.4	39.5	20.6	–147.8	–148.5
L10	**R16**	**N1**	67.0	54.0	20.6	–146.2	–141.6
L10	**R20**	**N1**	67.0	55.9	20.6	–142.4	–143.5
L10	**R5**	**N1**	67.0	50.4	20.6	–139.5	–138.0
L10	**R11**	**N1**	67.0	48.5	20.6	–137.5	–136.1
L10	**R40**	**N1**	67.0	52.1	20.6	–135.5	–139.7
L10	**R48**	**N1**	67.0	53.1	20.6	–135.7	–140.7
L10	**R1**	**N1**	67.0	46.4	20.6	–134.2	–134.0
L10	**R12**	**N1**	67.0	41.1	20.6	–126.8	–128.7
L10	**R95**	**N1**	67.0	42.8	20.6	not located	–130.4
L10	**R6**	**N1**	67.0	39.5	20.6	–125.4	–127.1
L4	**R16**	**N1**	80.0	54.0	20.6	–155.2	–154.6
L4	**R20**	**N1**	80.0	55.9	20.6	–158.8	–156.5

L4	**R5**	**N1**	80.0	50.4	20.6	–152.6	–151.0
L4	**R11**	**N1**	80.0	48.5	20.6	–149.0	–149.1
L4	**R40**	**N1**	80.0	52.1	20.6	–151.7	–152.7
L4	**R48**	**N1**	80.0	53.1	20.6	–155.5	–153.7
L4	**R1**	**N1**	80.0	46.4	20.6	–145.4	–147.0
L4	**R12**	**N1**	80.0	41.1	20.6	–140.7	–141.7
L4	**R95**	**N1**	80.0	42.8	20.6	–144.8	–143.4
L4	**R6**	**N1**	80.0	39.5	20.6	–136.7	–140.1
L6	**R16**	**N7**	83.7	54.0	–3.9	–131.8	–133.8
L6	**R20**	**N7**	83.7	55.9	–3.9	not located	–135.7
L6	**R5**	**N7**	83.7	50.4	–3.9	–130.7	–130.2
L6	**R11**	**N7**	83.7	48.5	–3.9	–128.8	–128.3
L6	**R40**	**N7**	83.7	52.1	–3.9	–133.3	–131.9
L6	**R48**	**N7**	83.7	53.1	–3.9	not located	–132.9
L6	**R1**	**N7**	83.7	46.4	–3.9	–127.3	–126.2
L6	**R12**	**N7**	83.7	41.1	–3.9	–118.4	–120.9
L6	**R95**	**N7**	83.7	42.8	–3.9	not located	–122.6
L6	**R6**	**N7**	83.7	39.5	–3.9	–120.1	–119.3
L7	**R16**	**N7**	112.3	54.0	–3.9	–160.3	–162.4
L7	**R20**	**N7**	112.3	55.9	–3.9	not located	–164.3
L7	**R5**	**N7**	112.3	50.4	–3.9	–159.2	–158.8
L7	**R11**	**N7**	112.3	48.5	–3.9	–156.4	–156.9
L7	**R40**	**N7**	112.3	52.1	–3.9	–163.0	–160.5
L7	**R48**	**N7**	112.3	53.1	–3.9	not located	–161.5
L7	**R1**	**N7**	112.3	46.4	–3.9	–156.7	–154.8
L7	**R12**	**N7**	112.3	41.1	–3.9	–148.4	–149.5
L7	**R95**	**N7**	112.3	42.8	–3.9	not located	–151.2
L7	**R6**	**N7**	112.3	39.5	–3.9	–151.8	–147.9
L14	**R16**	**N7**	88.4	54.0	–3.9	–138.6	–138.5
L14	**R20**	**N7**	88.4	55.9	–3.9	not located	–140.4
L14	**R5**	**N7**	88.4	50.4	–3.9	–135.9	–134.9
L14	**R11**	**N7**	88.4	48.5	–3.9	–134.0	–133.0
L14	**R40**	**N7**	88.4	52.1	–3.9	–138.4	–136.6
L14	**R48**	**N7**	88.4	53.1	–3.9	not located	–137.6
L14	**R1**	**N7**	88.4	46.4	–3.9	–132.6	–130.9
L14	**R12**	**N7**	88.4	41.1	–3.9	–124.9	–125.6
L14	**R95**	**N7**	88.4	42.8	–3.9	not located	–127.3
L14	**R6**	**N7**	88.4	39.5	–3.9	not located	–124.0
L10	**R16**	**N7**	67.0	54.0	–3.9	–114.0	–117.1

L10	**R20**	**N7**	67.0	55.9	–3.9	not located	–119.0
L10	**R5**	**N7**	67.0	50.4	–3.9	–109.8	–113.5
L10	**R11**	**N7**	67.0	48.5	–3.9	–107.6	–111.6
L10	**R40**	**N7**	67.0	52.1	–3.9	–114.2	–115.2
L10	**R48**	**N7**	67.0	53.1	–3.9	not located	–116.2
L10	**R1**	**N7**	67.0	46.4	–3.9	–106.5	–109.5
L10	**R12**	**N7**	67.0	41.1	–3.9	–101.6	–104.2
L10	**R95**	**N7**	67.0	42.8	–3.9	not located	–105.9
L10	**R6**	**N7**	67.0	39.5	–3.9	–104.2	–102.6
L4	**R16**	**N7**	80.0	54.0	–3.9	–128.5	–130.1
L4	**R20**	**N7**	80.0	55.9	–3.9	–132.4	–132.0
L4	**R5**	**N7**	80.0	50.4	–3.9	–126.4	–126.5
L4	**R11**	**N7**	80.0	48.5	–3.9	–125.0	–124.6
L4	**R40**	**N7**	80.0	52.1	–3.9	–130.0	–128.2
L4	**R48**	**N7**	80.0	53.1	–3.9	not located	–129.2
L4	**R1**	**N7**	80.0	46.4	–3.9	–124.0	–122.5
L4	**R12**	**N7**	80.0	41.1	–3.9	–117.2	–117.2
L4	**R95**	**N7**	80.0	42.8	–3.9	not located	–118.9
L4	**R6**	**N7**	80.0	39.5	–3.9	–117.6	–115.6
L6	**R16**	**N2**	83.7	54.0	18.9	–155.9	–156.6
L6	**R20**	**N2**	83.7	55.9	18.9	–158.0	–158.5
L6	**R5**	**N2**	83.7	50.4	18.9	–151.8	–153.0
L6	**R11**	**N2**	83.7	48.5	18.9	–151.6	–151.1
L6	**R40**	**N2**	83.7	52.1	18.9	–154.2	–154.7
L6	**R48**	**N2**	83.7	53.1	18.9	not located	–155.7
L6	**R1**	**N2**	83.7	46.4	18.9	–147.0	–149.0
L6	**R12**	**N2**	83.7	41.1	18.9	–143.7	–143.7
L6	**R95**	**N2**	83.7	42.8	18.9	not located	–145.4
L6	**R6**	**N2**	83.7	39.5	18.9	–138.3	–142.1
L7	**R16**	**N2**	112.3	54.0	18.9	–183.9	–185.2
L7	**R20**	**N2**	112.3	55.9	18.9	–188.7	–187.1
L7	**R5**	**N2**	112.3	50.4	18.9	–182.0	–181.6
L7	**R11**	**N2**	112.3	48.5	18.9	–180.0	–179.7
L7	**R40**	**N2**	112.3	52.1	18.9	–182.6	–183.3
L7	**R48**	**N2**	112.3	53.1	18.9	not located	–184.3
L7	**R1**	**N2**	112.3	46.4	18.9	–178.4	–177.6
L7	**R12**	**N2**	112.3	41.1	18.9	–175.5	–172.3
L7	**R95**	**N2**	112.3	42.8	18.9	not located	–174.0
L7	**R6**	**N2**	112.3	39.5	18.9	–171.7	–170.7

L14	**R16**	**N2**	88.4	54.0	18.9	–162.1	–161.3
L14	**R20**	**N2**	88.4	55.9	18.9	–162.0	–163.2
L14	**R5**	**N2**	88.4	50.4	18.9	–157.1	–157.7
L14	**R11**	**N2**	88.4	48.5	18.9	–156.7	–155.8
L14	**R40**	**N2**	88.4	52.1	18.9	–158.4	–159.4
L14	**R48**	**N2**	88.4	53.1	18.9	not located	–160.4
L14	**R1**	**N2**	88.4	46.4	18.9	–153.1	–153.7
L14	**R12**	**N2**	88.4	41.1	18.9	–151.1	–148.4
L14	**R95**	**N2**	88.4	42.8	18.9	not located	–150.1
L14	**R6**	**N2**	88.4	39.5	18.9	–146.9	–146.8
L10	**R16**	**N2**	67.0	54.0	18.9	–144.1	–139.9
L10	**R20**	**N2**	67.0	55.9	18.9	–142.7	–141.8
L10	**R5**	**N2**	67.0	50.4	18.9	–136.1	–136.3
L10	**R11**	**N2**	67.0	48.5	18.9	–133.9	–134.4
L10	**R40**	**N2**	67.0	52.1	18.9	–135.1	–138.0
L10	**R48**	**N2**	67.0	53.1	18.9	–135.8	–139.0
L10	**R1**	**N2**	67.0	46.4	18.9	–130.5	–132.3
L10	**R12**	**N2**	67.0	41.1	18.9	–128.8	–127.0
L10	**R95**	**N2**	67.0	42.8	18.9	–129.9	–128.7
L10	**R6**	**N2**	67.0	39.5	18.9	–125.6	–125.4
L4	**R16**	**N2**	80.0	54.0	18.9	–152.2	–152.9
L4	**R20**	**N2**	80.0	55.9	18.9	–157.0	–154.8
L4	**R5**	**N2**	80.0	50.4	18.9	–147.5	–149.3
L4	**R11**	**N2**	80.0	48.5	18.9	–148.3	–147.4
L4	**R40**	**N2**	80.0	52.1	18.9	–145.8	–151.0
L4	**R48**	**N2**	80.0	53.1	18.9	–154.0	–152.0
L4	**R1**	**N2**	80.0	46.4	18.9	–146.3	–145.3
L4	**R12**	**N2**	80.0	41.1	18.9	–141.4	–140.0
L4	**R95**	**N2**	80.0	42.8	18.9	not located	–141.7
L4	**R6**	**N2**	80.0	39.5	18.9	–138.5	–138.4

Supplementary Table 15: Free energy changes for radical substitution transition states (RS-TS) of reactions for constructing LFERs in Fig. 3a of the main text. a, free energy changes of RS-TS obtained from DFT calculations. **b,** free energy barriers of RS-TS predicted by the LFER model in Fig. 3d of the main text.

Ligands	Radicals	Nucleophiles	L_{RS}	R_{RS}	N_{RS}	$\Delta G^{\ddagger}_{RS}$(calc.)[a] (kcal/mol)	$\Delta G^{\ddagger}_{RS}$(pred.)[b] (kcal/mol)
L6	**R16**	**N10**	40.3	11.3	62.3	–113.4	–113.9
L6	**R16**	**N1**	40.3	11.3	92.3	not located	–143.9
L6	**R16**	**N7**	40.3	11.3	73.9	–124.7	–125.5
L6	**R16**	**N2**	40.3	11.3	88.8	–137.9	–140.4

L7	**R16**	**N10**	61.1	11.3	62.3	–133.2	–134.7
L7	**R16**	**N1**	61.1	11.3	92.3	not located	–164.7
L7	**R16**	**N7**	61.1	11.3	73.9	–145.6	–146.3
L7	**R16**	**N2**	61.1	11.3	88.8	–161.1	–161.2
L14	**R16**	**N10**	52.0	11.3	62.3	–128.1	–125.6
L14	**R16**	**N1**	52.0	11.3	92.3	not located	–155.6
L14	**R16**	**N7**	52.0	11.3	73.9	–141.4	–137.2
L14	**R16**	**N2**	52.0	11.3	88.8	not located	–152.1
L10	**R16**	**N10**	16.6	11.3	62.3	not located	–90.2
L10	**R16**	**N1**	16.6	11.3	92.3	not located	–120.2
L10	**R16**	**N7**	16.6	11.3	73.9	not located	–101.8
L10	**R16**	**N2**	16.6	11.3	88.8	not located	–116.7
L4	**R16**	**N10**	35.1	11.3	62.3	–108.5	–108.7
L4	**R16**	**N1**	35.1	11.3	92.3	–138.7	–138.7
L4	**R16**	**N7**	35.1	11.3	73.9	–119.0	–120.3
L4	**R16**	**N2**	35.1	11.3	88.8	–135.9	–135.2
L6	**R5**	**N10**	40.3	9.7	62.3	–113.3	–112.3
L6	**R5**	**N1**	40.3	9.7	92.3	not located	–142.3
L6	**R5**	**N7**	40.3	9.7	73.9	–123.6	–123.9
L6	**R5**	**N2**	40.3	9.7	88.8	not located	–138.8
L7	**R5**	**N10**	61.1	9.7	62.3	not located	–133.1
L7	**R5**	**N1**	61.1	9.7	92.3	not located	–163.1
L7	**R5**	**N7**	61.1	9.7	73.9	not located	–144.7
L7	**R5**	**N2**	61.1	9.7	88.8	not located	–159.6
L14	**R5**	**N10**	52.0	9.7	62.3	not located	–124.0
L14	**R5**	**N1**	52.0	9.7	92.3	not located	–154.0
L14	**R5**	**N7**	52.0	9.7	73.9	–135.6	–135.6
L14	**R5**	**N2**	52.0	9.7	88.8	not located	–150.5
L10	**R5**	**N10**	16.6	9.7	62.3	not located	–88.6
L10	**R5**	**N1**	16.6	9.7	92.3	not located	–118.6
L10	**R5**	**N7**	16.6	9.7	73.9	not located	–100.2
L10	**R5**	**N2**	16.6	9.7	88.8	not located	–115.1
L4	**R5**	**N10**	35.1	9.7	62.3	–107.6	–107.1
L4	**R5**	**N1**	35.1	9.7	92.3	not located	–137.1
L4	**R5**	**N7**	35.1	9.7	73.9	–115.7	–118.7
L4	**R5**	**N2**	35.1	9.7	88.8	–135.5	–133.6
L6	**R11**	**N10**	40.3	10.8	62.3	–112.4	–113.4
L6	**R11**	**N1**	40.3	10.8	92.3	not located	–143.4
L6	**R11**	**N7**	40.3	10.8	73.9	–124.3	–125.0

L6	**R11**	**N2**	40.3	10.8	88.8	–138.5	–139.9
L7	**R11**	**N10**	61.1	10.8	62.3	–133.0	–134.2
L7	**R11**	**N1**	61.1	10.8	92.3	–166.2	–164.2
L7	**R11**	**N7**	61.1	10.8	73.9	–147.3	–145.8
L7	**R11**	**N2**	61.1	10.8	88.8	–163.0	–160.7
L14	**R11**	**N10**	52.0	10.8	62.3	–125.8	–125.1
L14	**R11**	**N1**	52.0	10.8	92.3	not located	–155.1
L14	**R11**	**N7**	52.0	10.8	73.9	–138.1	–136.7
L14	**R11**	**N2**	52.0	10.8	88.8	–150.6	–151.6
L10	**R11**	**N10**	16.6	10.8	62.3	not located	–89.7
L10	**R11**	**N1**	16.6	10.8	92.3	not located	–119.7
L10	**R11**	**N7**	16.6	10.8	73.9	not located	–101.3
L10	**R11**	**N2**	16.6	10.8	88.8	not located	–116.2
L4	**R11**	**N10**	35.1	10.8	62.3	–106.6	–108.2
L4	**R11**	**N1**	35.1	10.8	92.3	not located	–138.2
L4	**R11**	**N7**	35.1	10.8	73.9	–119.3	–119.8
L4	**R11**	**N2**	35.1	10.8	88.8	–133.3	–134.7
L6	**R1**	**N10**	40.3	9.6	62.3	–114.7	–112.2
L6	**R1**	**N1**	40.3	9.6	92.3	not located	–142.2
L6	**R1**	**N7**	40.3	9.6	73.9	–124.7	–123.8
L6	**R1**	**N2**	40.3	9.6	88.8	–136.9	–138.7
L7	**R1**	**N10**	61.1	9.6	62.3	not located	–133.0
L7	**R1**	**N1**	61.1	9.6	92.3	not located	–163.0
L7	**R1**	**N7**	61.1	9.6	73.9	not located	–144.6
L7	**R1**	**N2**	61.1	9.6	88.8	not located	–159.5
L14	**R1**	**N10**	52.0	9.6	62.3	–122.2	–123.9
L14	**R1**	**N1**	52.0	9.6	92.3	not located	–153.9
L14	**R1**	**N7**	52.0	9.6	73.9	–135.1	–135.5
L14	**R1**	**N2**	52.0	9.6	88.8	not located	–150.4
L10	**R1**	**N10**	16.6	9.6	62.3	not located	–88.5
L10	**R1**	**N1**	16.6	9.6	92.3	not located	–118.5
L10	**R1**	**N7**	16.6	9.6	73.9	not located	–100.1
L10	**R1**	**N2**	16.6	9.6	88.8	not located	–115.0
L4	**R1**	**N10**	35.1	9.6	62.3	–106.6	–107.0
L4	**R1**	**N1**	35.1	9.6	92.3	–137.2	–137.0
L4	**R1**	**N7**	35.1	9.6	73.9	–116.4	–118.6
L4	**R1**	**N2**	35.1	9.6	88.8	–135.7	–133.5
L6	**R12**	**N10**	40.3	8.5	62.3	–112.6	–111.1
L6	**R12**	**N1**	40.3	8.5	92.3	not located	–141.1

L6	**R12**	**N7**	40.3	8.5	73.9	–122.4	–122.7
L6	**R12**	**N2**	40.3	8.5	88.8	–137.5	–137.6
L7	**R12**	**N10**	61.1	8.5	62.3	–129.7	–131.9
L7	**R12**	**N1**	61.1	8.5	92.3	–159.7	–161.9
L7	**R12**	**N7**	61.1	8.5	73.9	–144.4	–143.5
L7	**R12**	**N2**	61.1	8.5	88.8	–159.6	–158.4
L14	**R12**	**N10**	52.0	8.5	62.3	–121.9	–122.8
L14	**R12**	**N1**	52.0	8.5	92.3	not located	–152.8
L14	**R12**	**N7**	52.0	8.5	73.9	–136.1	–134.4
L14	**R12**	**N2**	52.0	8.5	88.8	–145.3	–149.3
L10	**R12**	**N10**	16.6	8.5	62.3	not located	–87.4
L10	**R12**	**N1**	16.6	8.5	92.3	not located	–117.4
L10	**R12**	**N7**	16.6	8.5	73.9	not located	–99.0
L10	**R12**	**N2**	16.6	8.5	88.8	not located	–113.9
L4	**R12**	**N10**	35.1	8.5	62.3	–106.9	–105.9
L4	**R12**	**N1**	35.1	8.5	92.3	not located	–135.9
L4	**R12**	**N7**	35.1	8.5	73.9	–118.4	–117.5
L4	**R12**	**N2**	35.1	8.5	88.8	–135.0	–132.4
L6	**R6**	**N10**	40.3	9.2	62.3	–114.5	–111.8
L6	**R6**	**N1**	40.3	9.2	92.3	not located	–141.8
L6	**R6**	**N7**	40.3	9.2	73.9	–124.2	–123.4
L6	**R6**	**N2**	40.3	9.2	88.8	–137.3	–138.3
L7	**R6**	**N10**	61.1	9.2	62.3	not located	–132.6
L7	**R6**	**N1**	61.1	9.2	92.3	not located	–162.6
L7	**R6**	**N7**	61.1	9.2	73.9	not located	–144.2
L7	**R6**	**N2**	61.1	9.2	88.8	not located	–159.1
L14	**R6**	**N10**	52.0	9.2	62.3	–121.5	–123.5
L14	**R6**	**N1**	52.0	9.2	92.3	not located	–153.5
L14	**R6**	**N7**	52.0	9.2	73.9	–134.3	–135.1
L14	**R6**	**N2**	52.0	9.2	88.8	not located	–150.0
L10	**R6**	**N10**	16.6	9.2	62.3	not located	–88.1
L10	**R6**	**N1**	16.6	9.2	92.3	not located	–118.1
L10	**R6**	**N7**	16.6	9.2	73.9	–99.7	–99.7
L10	**R6**	**N2**	16.6	9.2	88.8	not located	–114.6
L4	**R6**	**N10**	35.1	9.2	62.3	–106.5	–106.6
L4	**R6**	**N1**	35.1	9.2	92.3	not located	–136.6
L4	**R6**	**N7**	35.1	9.2	73.9	–116.3	–118.2
L4	**R6**	**N2**	35.1	9.2	88.8	–134.6	–133.1

Supplementary Table 16: Free energy changes for ion pair-type bond formation transition states (IP-TS) of reactions for

constructing LFER in Fig. 3a of the main text. a, free energy changes of IP-TS obtained from DFT calculations. **b,** free energy barriers of IP-TS predicted by the LFER model in Fig. 3e of the main text.

Ligands	Radicals	Nucleophiles	L_{IP}	R_{IP}	N_{IP}	$\Delta G^{\ddagger}_{IP}$(calc.)[a] (kcal/mol)	$\Delta G^{\ddagger}_{IP}$(pred.)[b] (kcal/mol)
L6	**R20**	**N10**	56.6	73.5	5.1	–137.5	–135.2
L6	**R20**	**N61**	56.6	73.5	31.4	not located	–161.5
L6	**R20**	**N1**	56.6	73.5	27.0	not located	–157.1
L6	**R20**	**N7**	56.6	73.5	17.4	not located	–147.5
L6	**R20**	**N2**	56.6	73.5	26.1	not located	–156.2
L6	**R48**	**N10**	56.6	76.9	5.1	–140.3	–138.6
L6	**R48**	**N61**	56.6	76.9	31.4	not located	–164.9
L6	**R48**	**N1**	56.6	76.9	27.0	–161.5	–160.5
L6	**R48**	**N7**	56.6	76.9	17.4	–149.7	–150.9
L6	**R48**	**N2**	56.6	76.9	26.1	–158.9	–159.6
L6	**R95**	**N10**	56.6	73.4	5.1	–137.7	–135.1
L6	**R95**	**N61**	56.6	73.4	31.4	–159.9	–161.4
L6	**R95**	**N1**	56.6	73.4	27.0	–157.4	–157.0
L6	**R95**	**N7**	56.6	73.4	17.4	–147.1	–147.4
L6	**R95**	**N2**	56.6	73.4	26.1	–151.7	–156.1
L6	**R6**	**N10**	56.6	48.6	5.1	not located	–110.3
L6	**R6**	**N61**	56.6	48.6	31.4	not located	–136.6
L6	**R6**	**N1**	56.6	48.6	27.0	not located	–132.2
L6	**R6**	**N7**	56.6	48.6	17.4	not located	–122.6
L6	**R6**	**N2**	56.6	48.6	26.1	not located	–131.3
L7	**R20**	**N10**	84.4	73.5	5.1	–160.2	–163.0
L7	**R20**	**N61**	84.4	73.5	31.4	not located	–189.3
L7	**R20**	**N1**	84.4	73.5	27.0	not located	–184.9
L7	**R20**	**N7**	84.4	73.5	17.4	–177.2	–175.3
L7	**R20**	**N2**	84.4	73.5	26.1	not located	–184.0
L7	**R48**	**N10**	84.4	76.9	5.1	–161.9	–166.4
L7	**R48**	**N61**	84.4	76.9	31.4	not located	–192.7
L7	**R48**	**N1**	84.4	76.9	27.0	–189.2	–188.3
L7	**R48**	**N7**	84.4	76.9	17.4	–178.5	–178.7
L7	**R48**	**N2**	84.4	76.9	26.1	–189.2	–187.4
L7	**R95**	**N10**	84.4	73.4	5.1	–159.8	–162.9
L7	**R95**	**N61**	84.4	73.4	31.4	not located	–189.2
L7	**R95**	**N1**	84.4	73.4	27.0	–185.6	–184.8
L7	**R95**	**N7**	84.4	73.4	17.4	–176.6	–175.2
L7	**R95**	**N2**	84.4	73.4	26.1	–187.2	–183.9

L7	**R6**	**N10**	84.4	48.6	5.1	–138.6	–138.1
L7	**R6**	**N61**	84.4	48.6	31.4	not located	–164.4
L7	**R6**	**N1**	84.4	48.6	27.0	not located	–160.0
L7	**R6**	**N7**	84.4	48.6	17.4	not located	–150.4
L7	**R6**	**N2**	84.4	48.6	26.1	not located	–159.1
L14	**R20**	**N10**	58.0	73.5	5.1	–135.3	–136.6
L14	**R20**	**N61**	58.0	73.5	31.4	not located	–162.9
L14	**R20**	**N1**	58.0	73.5	27.0	not located	–158.5
L14	**R20**	**N7**	58.0	73.5	17.4	–148.1	–148.9
L14	**R20**	**N2**	58.0	73.5	26.1	not located	–157.6
L14	**R48**	**N10**	58.0	76.9	5.1	–137.6	–140.0
L14	**R48**	**N61**	58.0	76.9	31.4	–168.4	–166.3
L14	**R48**	**N1**	58.0	76.9	27.0	–162.1	–161.9
L14	**R48**	**N7**	58.0	76.9	17.4	–151.1	–152.3
L14	**R48**	**N2**	58.0	76.9	26.1	–160.9	–161.0
L14	**R95**	**N10**	58.0	73.4	5.1	–136.8	–136.5
L14	**R95**	**N61**	58.0	73.4	31.4	–163.3	–162.8
L14	**R95**	**N1**	58.0	73.4	27.0	–157.9	–158.4
L14	**R95**	**N7**	58.0	73.4	17.4	–150.0	–148.8
L14	**R95**	**N2**	58.0	73.4	26.1	–158.7	–157.5
L14	**R6**	**N10**	58.0	48.6	5.1	not located	–111.7
L14	**R6**	**N61**	58.0	48.6	31.4	not located	–138.0
L14	**R6**	**N1**	58.0	48.6	27.0	not located	–133.6
L14	**R6**	**N7**	58.0	48.6	17.4	not located	–124.0
L14	**R6**	**N2**	58.0	48.6	26.1	not located	–132.7
L10	**R20**	**N10**	40.6	73.5	5.1	–118.1	–119.2
L10	**R20**	**N61**	40.6	73.5	31.4	not located	–145.5
L10	**R20**	**N1**	40.6	73.5	27.0	not located	–141.1
L10	**R20**	**N7**	40.6	73.5	17.4	not located	–131.5
L10	**R20**	**N2**	40.6	73.5	26.1	not located	–140.2
L10	**R48**	**N10**	40.6	76.9	5.1	–125.7	–122.6
L10	**R48**	**N61**	40.6	76.9	31.4	not located	–148.9
L10	**R48**	**N1**	40.6	76.9	27.0	–146.2	–144.5
L10	**R48**	**N7**	40.6	76.9	17.4	not located	–134.9
L10	**R48**	**N2**	40.6	76.9	26.1	–142.1	–143.6
L10	**R95**	**N10**	40.6	73.4	5.1	–120.6	–119.1
L10	**R95**	**N61**	40.6	73.4	31.4	–146.4	–145.4
L10	**R95**	**N1**	40.6	73.4	27.0	–136.0	–141.0
L10	**R95**	**N7**	40.6	73.4	17.4	–131.8	–131.4

L10	**R95**	**N2**	40.6	73.4	26.1	not located	–140.1
L10	**R6**	**N10**	40.6	48.6	5.1	not located	–94.3
L10	**R6**	**N61**	40.6	48.6	31.4	not located	–120.6
L10	**R6**	**N1**	40.6	48.6	27.0	not located	–116.2
L10	**R6**	**N7**	40.6	48.6	17.4	not located	–106.6
L10	**R6**	**N2**	40.6	48.6	26.1	not located	–115.3
L4	**R20**	**N10**	54.6	73.5	5.1	–135.1	–133.2
L4	**R20**	**N61**	54.6	73.5	31.4	not located	–159.5
L4	**R20**	**N1**	54.6	73.5	27.0	not located	–155.1
L4	**R20**	**N7**	54.6	73.5	17.4	–145.6	–145.5
L4	**R20**	**N2**	54.6	73.5	26.1	not located	–154.2
L4	**R48**	**N10**	54.6	76.9	5.1	–137.3	–136.6
L4	**R48**	**N61**	54.6	76.9	31.4	not located	–162.9
L4	**R48**	**N1**	54.6	76.9	27.0	–157.9	–158.5
L4	**R48**	**N7**	54.6	76.9	17.4	–147.4	–148.9
L4	**R48**	**N2**	54.6	76.9	26.1	not located	–157.6
L4	**R95**	**N10**	54.6	73.4	5.1	–133.9	–133.1
L4	**R95**	**N61**	54.6	73.4	31.4	–157.1	–159.4
L4	**R95**	**N1**	54.6	73.4	27.0	–156.0	–155.0
L4	**R95**	**N7**	54.6	73.4	17.4	–145.2	–145.4
L4	**R95**	**N2**	54.6	73.4	26.1	–154.3	–154.1
L4	**R6**	**N10**	54.6	48.6	5.1	–107.8	–108.3
L4	**R6**	**N61**	54.6	48.6	31.4	not located	–134.6
L4	**R6**	**N1**	54.6	48.6	27.0	not located	–130.2
L4	**R6**	**N7**	54.6	48.6	17.4	not located	–120.6
L4	**R6**	**N2**	54.6	48.6	26.1	not located	–129.3

4.3 LFER Parameter Scaling Method

We developed a more efficient method to replace the least squares approach used in the main text and Section 4.2 of the Supplementary Information. This new method involves selecting optimal ligand-radical-nucleophile combinations for each mechanism (denoted as **L0**, **R0**, **N0**) as reference to derive the LFER parameters for additional ligands (**Lx**), radicals (**Rx**), and nucleophiles (**Nx**). For instance, to determine the LFER parameter **Lx** for a ligand in a specific bond formation mechanism, we calculate the free energy change of the bond formation transition state for the combination **Lx**, **R0**, **N0** ($\Delta G^{\ddagger}_{x,0,0}$), subtract the free energy change of the reference combination ($\Delta G^{\ddagger}_{0,0,0}$), and add the LFER parameter of the reference ligand (L_0), as outlined in *eq5* of Supplementary Figure 14. Similarly, the LFER parameters for other radicals (R_x) and nucleophiles (N_x) can be derived using *eq6* and *eq7*, respectively.

$$\begin{aligned}
\Delta G^{\ddagger}_{0,0,0} &= L_0 + R_0 + N_0 \ (eq1) \\
\Delta G^{\ddagger}_{x,0,0} &= L_x + R_0 + N_0 \ (eq2) \\
\Delta G^{\ddagger}_{0,x,0} &= L_0 + R_x + N_0 \ (eq3) \\
\Delta G^{\ddagger}_{0,0,x} &= L_0 + R_0 + N_x \ (eq4)
\end{aligned}
\quad \Rightarrow \quad
\begin{aligned}
L_x &= \Delta G^{\ddagger}_{x,0,0} - \Delta G_{0,0,0} + L_0 \ (eq5) \\
R_x &= \Delta G^{\ddagger}_{0,x,0} - \Delta G_{0,0,0} + R_0 \ (eq6) \\
N_x &= \Delta G^{\ddagger}_{0,0,x} - \Delta G_{0,0,0} + N_0 \ (eq7)
\end{aligned}$$

Supplementary Figure 14: Another approach for generating LFER parameters. *eq1*, the reference combination of ligand (L_0), radical (R_0), and nucleophile (N_0). *eq2-4*, while two components keeping constant, free energy barriers of transition states for different bond formation mechanisms where either other component changed (*Lx*, ligand; R_x, radical; N_x, nucleophile) are calculated. *eq5-7*, generating reaction parameters for ligands, radicals, and nucleophiles absent from the selected scope in Fig. 3a by subtraction between *eq1* and *eq2-4*.

Supplementary Table 17: Correlation results of the optimal combination reference between parameters-fit and parameters-subtraction for bond formation processes.

We compared the correlation between the LFER parameters generated using the least squares method (termed "parameters-LSM") and those derived from the subtraction-based equation in Supplementary Figure 14 (termed "parameters-subtraction"). Based on a comprehensive evaluation of the correlation coefficient between parameters-LSM and parameters-subtraction, as well as the computational feasibility of DFT calculations, we selected the optimal combination of reference compounds. For clarity and readability, Supplementary Table 17 presents only the performance of the optimal ligand-radical-nucleophile combinations as references for different bond formation processes. The standard error and coefficient of determination (R^2) quantify the statistical equivalence between the parameters-LSM and parameters-subtraction. The complete performance data for all combinations across different bond formation processes are available at GitHub: https://github.com/XuGuoXiong/LFER-on-Mechanism-Prediction.git.

Entry	Mechanism	Ligand	Radical	Nucleophile	Correlation Coefficient			Correlation Result	
					Pearson	Kendall	Spearman	Standard Error (kcal/mol)	R^2
1	RE	**L4**	**R11**	**N61**	0.997	0.958	0.991	0.019	0.997
2	RS	**L4**	**R16**	**N7**	0.999	0.868	0.956	0.014	0.999
3	IP	**L4**	**R94**	**N10**	0.998	0.978	0.996	0.018	0.998

The combination of the BOX ligand (**L4**), the secondary α-acyl radical (**R11**), and the methyl anion (**N61**) was selected as the reference for the reductive elimination process (Entry 1), as this nucleophile facilitates the localization of reductive elimination transition states. For the radical substitution process (Entry 2), the combination of the BOX ligand (**L4**), the primary α-acyl radical (**R16**), and the phenylethynyl anion (**N7**) was chosen as the reference. The combination of the BOX ligand (**L4**), the tertiary α-amino radical (**R94**), and the cyanide anion (**N10**) was selected as the reference for the ion pair-type bond formation process (Entry 3).

4.4 Reactions for Testing LFER.

Supplementary Table 18 to Supplementary Table 20 present the free energy changes of reductive elimination (RE), radical substitution (RS), and ion pair-type bond formation (IP) processes for reactions for testing LFER in Fig. 3a of the main text. These parameters were generated using the method described in Section 4.3. Each table includes the following columns: ligand numbering, radical numbering, nucleophile numbering, LFER parameters for ligands, LFER parameters for radicals, LFER parameters for nucleophiles, free energy changes of bond formation processes obtained from DFT calculations, and free energy changes predicted by the LFER model. According to our LFER model, the free energy changes of bond formation processes can be predicted by summing the LFER parameters of the ligand, radical, and nucleophile for the corresponding mechanism.

Supplementary Table 18: Free energy changes for reductive elimination transition states (RE-TS) of reactions for testing LFER in Fig. 3c of the main text. a, free energy changes of RE-TS obtained from DFT calculations. **b,** free energy changes of RE-TS predicted by the LFER model in Fig. 3c of the main text.

Ligands	Radicals	Nucleophiles	L_{RE}	R_{RE}	N_{RE}	$\Delta G^{\ddagger}_{RE}$(calc.)[a] (kcal/mol)	$\Delta G^{\ddagger}_{RE}$(pred.)[b] (kcal/mol)
L1	**R2**	**N18**	70.2	44.8	–6.2	–108.8	–108.8

L1	**R4**	**N64**	70.2	43.6	–24.3	–88.6	–89.4
L2	**R9**	**N23**	87.0	46.9	–20.0	–114.6	–113.9
L3	**R68**	**N10**	98.2	46.3	–17.4	–124.0	–127.1
L3	**R120**	**N22**	98.2	38.6	–17.8	–116.7	–118.9
L4	**R12**	**N75**	80.0	41.1	4.5	–121.8	–125.6
L4	**R17**	**N19**	80.0	57.8	–8.9	–124.4	–128.8
L4	**R27**	**N52**	80.0	50.0	16.7	–147.7	–146.6
L4	**R32**	**N11**	80.0	49.7	8.9	–137.1	–138.6
L4	**R43**	**N13**	80.0	51.2	–3.5	–128.0	–127.7
L4	**R44**	**N58**	80.0	51.7	–4.5	–125.5	–127.2
L4	**R51**	**N75**	80.0	43.4	4.5	–125.5	–127.9
L4	**R57**	**N32**	80.0	47.1	14.7	–139.2	–141.7
L4	**R62**	**N14**	80.0	47.2	–5.7	–119.5	–121.5
L4	**R65**	**N7**	80.0	46.4	–3.9	–123.4	–122.5
L4	**R82**	**N6**	80.0	43.8	23.3	–146.3	–147.1
L4	**R100**	**N35**	80.0	10.5	29.1	–116.8	–119.6
L4	**R105**	**N54**	80.0	41.9	22.0	–140.5	–143.9
L4	**R108**	**N56**	80.0	43.0	5.1	–126.9	–128.0
L4	**R123**	**N53**	80.0	37.1	15.2	–132.1	–132.4
L5	**R69**	**N10**	86.3	49.6	–17.4	–116.1	–118.5
L5	**R84**	**N1**	86.3	51.4	20.6	–159.8	–158.3
L7	**R86**	**N2**	112.3	44.4	18.9	–175.7	–175.5
L7	**R86**	**N7**	112.3	44.4	–3.9	–154.3	–152.7
L7	**R122**	**N10**	112.3	33.3	–17.4	–127.0	–128.1
L7	**R125**	**N17**	112.3	37.3	–8.3	–141.1	–141.3
L8	**R13**	**N10**	120.2	36.2	–17.4	–137.4	–139.0
L8	**R68**	**N24**	120.2	46.3	–2.8	–163.6	–163.7
L8	**R88**	**N10**	120.2	40.9	–17.4	–142.0	–143.7
L8	**R94**	**N61**	120.2	42.8	28.6	–194.4	–191.6
L9	**R20**	**N21**	136.9	55.9	0.3	–198.1	–193.2
L9	**R67**	**N15**	136.9	50.5	–7.0	–178.4	–180.4
L9	**R95**	**N15**	136.9	46.6	–7.0	–174.3	–176.6
L11	**R47**	**N11**	65.7	55.5	8.9	–124.6	–130.1
L13	**R3**	**N12**	65.6	41.9	–3.4	–106.9	–104.1
L13	**R87**	**N60**	65.6	41.3	3.0	–109.0	–109.9
L14	**R13**	**N35**	88.4	36.2	29.1	–153.8	–153.7
L14	**R107**	**N1**	88.4	36.3	20.6	–145.7	–145.3
L14	**R110**	**N32**	88.4	41.7	14.7	–142.8	–144.8
L14	**R119**	**N29**	88.4	38.7	19.8	–146.7	–146.9

L14	**R120**	**N2**	88.4	38.6	18.9	–146.0	–145.8

Supplementary Table 19: Free energy changes for radical substitution transition states (RS-TS) of reactions for testing LFER in Fig. 3d of the main text. a, free energy barriers of RS-TS calculated by DFT. **b,** free energy barriers of RS-TS predicted by the LFER model in Fig. 3d.

Ligands	Radicals	Nucleophiles	L_{RS}	R_{RS}	N_{RS}	$\Delta G^{\ddagger}_{RS}$(calc.)[a] (kcal/mol)	$\Delta G^{\ddagger}_{RS}$(pred.)[b] (kcal/mol)
L1	**R2**	**N18**	19.3	5.6	72.0	–95.4	–96.9
L2	**R10**	**N23**	40.5	6.8	60.7	–109.7	–108.0
L2	**R107**	**N20**	40.5	11.4	60.1	–110.2	–112.0
L3	**R68**	**N10**	45.3	9.2	62.3	–120.5	–116.8
L4	**R16**	**N5**	35.1	11.3	95.3	–141.6	–141.6
L4	**R23**	**N47**	35.1	7.0	80.1	–124.5	–122.2
L4	**R44**	**N58**	35.1	18.0	70.7	–120.3	–123.8
L4	**R45**	**N1**	35.1	10.9	92.3	–136.1	–138.3
L4	**R50**	**N48**	35.1	7.5	73.9	–113.8	–116.4
L4	**R53**	**N17**	35.1	8.4	70.3	–112.9	–113.7
L4	**R54**	**N30**	35.1	10.9	88.1	–133.6	–134.1
L4	**R114**	**N18**	35.1	11.1	72.0	–118.4	–118.2
L4	**R118**	**N31**	35.1	9.1	84.4	–129.2	–128.6
L4	**R124**	**N12**	35.1	11.3	74.5	–119.4	–120.8
L6	**R55**	**N58**	40.3	11.9	70.7	–122.6	–122.9
L7	**R120**	**N21**	61.1	15.3	77.1	–154.9	–153.5
L7	**R125**	**N17**	61.1	8.4	70.3	–141.3	–139.8
L8	**R13**	**N18**	69.8	10.0	72.0	–153.5	–151.8
L8	**R120**	**N11**	69.8	15.3	82.9	–166.3	–168.0
L13	**R7**	**N24**	32.9	11.8	74.7	–116.8	–119.4
L14	**R119**	**N29**	52.0	12.2	90.2	–150.2	–154.4
L3	**R68**	**N10**	45.3	9.2	62.3	–120.5	–116.8

Supplementary Table 20: Free energy changes for ion pair-type bond formation transition states (IP-TS) of reactions for testing LFER in Fig. 3e of the main text. a, free energy barriers of IP-TS calculated by DFT. **b,** free energy barriers of IP-TS predicted by the LFER model in Fig. 3e.

Ligands	Radicals	Nucleophiles	L_{IP}	R_{IP}	N_{IP}	$\Delta G^{\ddagger}_{IP}$ (calc.)[a] (kcal/mol)	$\Delta G^{\ddagger}_{IP}$ (pred.)[b] (kcal/mol)
L2	**R9**	**N23**	64.9	55.6	2.5	–123.0	–123.1
L2	**R10**	**N23**	64.9	49.4	2.5	–117.9	–116.8
L3	**R120**	**N22**	70.8	35.6	4.4	–108.9	–110.8
L4	**R20**	**N58**	54.6	73.5	8.4	–136.0	–136.5

L4	**R49**	**N11**	54.6	64.5	26.1	–145.3	–145.3
L4	**R67**	**N24**	54.6	62.6	16.1	–134.7	–133.3
L4	**R77**	**N17**	54.6	56.0	14.2	–123.7	–124.8
L4	**R100**	**N7**	54.6	31.2	17.4	–102.0	–103.2
L4	**R108**	**N56**	54.6	56.3	12.0	–126.2	–122.9
L4	**R116**	**N20**	54.6	47.6	3.1	–101.8	–105.3
L7	**R96**	**N11**	84.4	65.8	26.1	–174.2	–176.4
L7	**R122**	**N10**	84.4	40.0	5.1	–127.0	–129.5
L7	**R125**	**N17**	84.4	46.4	14.2	–147.9	–145.0
L9	**R94**	**N17**	102.0	73.4	14.2	–191.8	–189.5
L9	**R95**	**N15**	102.0	63.9	16.4	–180.6	–182.2
L13	**R87**	**N60**	41.4	46.4	15.3	–105.0	–103.1

5 Derivation of Missing R_{IP} and N_{RS} Parameters

Due to the tendency of highly unfavorable IP and RS bond formation processes to optimize into transition states of other bond formation mechanisms, the R_{IP} parameters for many radicals and the N_{RS} parameters for nucleophiles cannot be obtained through fitting or subtraction of bond formation transition state free energy changes (as shown in the main text and Supplementary Figure 14 in Section 4.3 of the Supplementary information). However, to quantitatively assess and compare the bond formation mechanism preferences of radicals and nucleophiles, as well as to map the mechanistic selectivity across a broad chemical space, we require an appropriate method to approximate these missing parameters.

We successfully developed two approaches to approximate R_{IP} and N_{RS} parameters. Inspired by the well-established multivariate linear regression (MLR) approach pioneered by Sigman et al.[21-23], we effectively derived R_{IP} parameters using MLR with conventional Physical Organic Properties (Section 5.1 and 5.2). Additionally, the high linear correlation between N_{RS} and N_{RE} provided a reliable alternative method for obtaining N_{RS} parameters (Section 5.3 and 5.4).

5.1 The Comparison between LFER Parameters and Physical Organic Properties of Radicals.

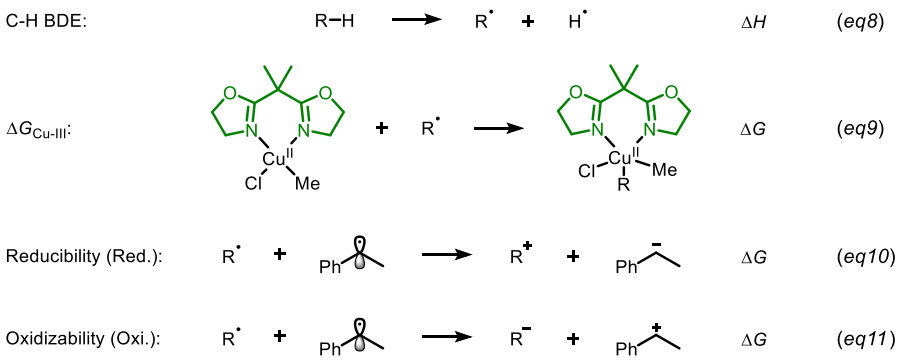

Supplementary Figure 15: The names and definitions of some Physical Organic Properties employed in Sections 5.1 and 5.2.

R_{IP} parameters for radicals and their correlations with conventional organic parameters are summarized in Supplementary Table 21. The results in Supplementary Table 22 indicate that the R_{IP} parameter is associated with the SOMO energy (E_{SOMO}), buried volume (BV), the affinity between radicals and Cu(II) complexes ($\Delta G_{Cu\text{-}III}$), single-electron reduction potential (Red.), and vertical ionization potential (VIP). These correlations allow the approximation of R_{IP} for radicals through multivariate linear regression (MLR) using these Physical

Organic Properties (see Supplementary Figure 16 in Section 5.2), providing an alternative approach to generate LFER parameters for radicals whose ion pair-type bond formation transition states could not be located. By predicting the free energy changes of ion pair-type bond formation processes using the MLR-generated R_{IP}, we further confirmed that the inability to locate these transition states often stems from the significantly lower favorability of the ion pair-type bond formation process compared to other bond formation mechanisms.

Supplementary Table 21: The comparison between LFER parameters and conventional Physical Organic Properties of radicals. ***E*$_{SOMO}$,** the energy of SOMO, values in kcal/mol. **ω,** the global electrophilicity index[24], values in kcal/mol. **BV(r=3),** the buried volume within a 3 Å radius of the radical bond formation atom center, values in %. **BDE**, the bond dissociation energy of the targeted C-H bond in the corresponding precursor of the radical *(eq8)*, values in kcal/mol. **Cu-III dG**, the free energy difference between radical-bonded Cu-III complex and the association of the corresponding free radical and Cu-II complex *(eq9)*, values in kcal/mol. **Charge**, the Mulliken charge distribution on the radical center atom. **Spin**, the Mulliken spin population on the radical center atom. **Red.**, reducibility of radicals determined by *eq10*, values in kcal/mol. **Oxi.**, oxidizability of radicals determined by *eq11*, values in kcal/mol. **VIP**, vertical ionization potential, values in kcal/mol. **VEA**, vertical electron affinity, values in kcal/mol.

Radicals	R_{IP}	E_{SOMO}	ω	BV(r=3)	BDE	$\Delta G_{Cu\text{-}III}$	Charge	Spin	Red.	Oxi.	VIP	VEA
R1	not located	–106.3	25.9	64.2	84.4	–5.8	–0.183	0.767	–6.0	–6.0	157.5	14.6
R2	not located	–119.9	26.7	57.5	84.1	–5.6	–0.269	0.778	–7.2	–6.1	183.4	9.4
R3	47.1	–111.8	22.6	61.3	80.7	–1.4	–0.094	0.659	–6.7	–6.4	172.4	2.8
R4	48.6	–104.5	33.1	68.7	79.7	–3.0	–0.296	0.656	–5.7	–5.4	148.6	29.1
R5	not located	–112.3	28.6	49.2	87.0	–9.9	–0.408	0.792	–6.4	–5.9	166.3	17.9
R6	48.6	–102.0	24.1	77.5	83.4	2.0	0.082	0.748	–5.7	–6.1	150.6	12.6
R7	not located	–126.9	46.7	64.3	82.3	–5.2	–0.171	0.714	–6.8	–4.7	176.2	45.1
R8	not located	–121.8	34.3	64.0	84.2	–5.9	–0.165	0.779	–6.7	–5.5	174.3	26.9
R9	55.6	–86.8	18.5	64.2	83.3	–6.6	–0.201	0.734	–4.8	–6.2	133.0	4.8
R10	49.4	–101.9	24.4	63.5	80.5	–3.2	–0.140	0.639	–5.9	–6.0	153.6	12.4
R11	not located	–142.9	36.5	61.4	89.8	–10.3	–0.121	0.893	–7.5	–5.4	205.0	24.6
R12	not located	–132.1	32.8	75.4	85.7	–1.6	0.113	0.830	–7.0	–5.6	189.6	20.8
R13	not located	–121.5	41.3	77.8	81.4	–0.3	0.013	0.667	–6.3	–5.0	169.4	38.5
R14	not located	–140.7	27.9	26.7	103.1	–17.3	–0.485	1.156	–9.2	–6.8	228.4	–1.8
R15	not located	–140.3	28.8	49.9	100.5	–16.2	–0.310	1.094	–8.2	–6.3	215.6	4.7
R16	not located	–159.9	43.3	45.8	95.8	–18.0	–0.327	0.968	–7.9	–5.1	228.5	32.2
R17	not located	–146.1	46.2	46.0	96.0	–18.4	–0.329	0.946	–8.1	–4.6	204.1	41.2
R18	not located	–136.1	42.1	51.2	95.9	–19.7	–0.352	0.960	–6.5	–4.8	195.0	36.2
R19	not located	–164.6	46.4	41.3	92.8	–15.6	–0.352	0.887	–9.6	–5.3	238.0	35.8
R20	73.5	–83.4	13.3	49.3	89.4	–17.7	–0.248	0.840	–4.9	–7.2	151.2	–17.1
R21	not located	–104.7	27.4	56.4	85.4	–8.8	–0.427	0.741	–5.8	–5.9	152.8	18.7
R22	not located	–107.2	29.0	69.0	85.0	–5.3	–0.439	0.738	–5.8	–5.8	152.8	21.6
R23	not located	–108.3	27.3	49.1	86.7	–10.2	–0.413	0.785	–6.0	–5.9	157.2	17.4
R24	not located	–118.6	33.4	51.8	87.9	–10.7	–0.406	0.780	–6.6	–5.5	170.0	26.0
R25	not located	–120.7	33.7	49.2	87.4	–11.1	–0.401	0.793	–6.7	–5.5	172.5	26.1

R26	not located	–116.7	31.9	49.2	86.8	–10.8	–0.408	0.779	–6.4	–5.6	166.9	24.1
R27	not located	–112.4	29.1	49.2	87.0	–10.0	–0.411	0.790	–6.5	–5.8	167.5	18.6
R28	not located	–118.3	33.0	49.2	87.0	–11.1	–0.406	0.783	–6.4	–5.5	167.4	26.0
R29	not located	–133.8	50.3	49.2	86.5	–9.9	–0.393	0.746	–7.2	–4.5	185.6	48.9
R30	56.7	–90.0	20.1	49.1	85.2	–9.6	–0.433	0.750	–5.1	–6.1	138.2	7.1
R31	not located	–110.2	31.7	49.2	86.3	–10.4	–0.413	0.751	–6.0	–5.6	157.3	25.4
R32	not located	–108.4	31.3	52.1	86.0	–9.9	–0.420	0.694	–6.0	–5.6	156.3	25.0
R33	not located	–121.9	33.7	47.9	88.5	–12.1	–0.359	0.804	–6.9	–5.6	177.0	25.2
R34	not located	–120.7	33.0	49.0	87.4	–10.4	–0.406	0.796	–6.8	–5.6	175.6	24.3
R35	not located	–129.6	37.9	48.9	88.2	–10.8	–0.386	0.812	–7.2	–5.3	185.1	31.0
R36	not located	–120.7	38.0	48.0	88.1	–14.4	–0.362	0.783	–6.5	–5.2	168.5	33.8
R37	not located	–119.0	37.9	50.7	87.6	–12.1	–0.358	0.714	–6.5	–5.2	167.6	33.8
R38	not located	–108.1	27.4	48.4	83.3	–7.7	–0.378	0.662	–6.3	–5.9	162.8	16.3
R39	not located	–110.3	25.2	48.1	87.2	–10.4	–0.404	0.787	–6.3	–6.2	165.2	11.0
R40	not located	–111.6	16.7	59.2	95.4	–11.3	–0.087	1.024	–6.6	–7.1	178.3	–16.8
R41	not located	–126.3	23.2	65.7	96.7	–13.0	–0.098	1.028	–7.3	–6.5	193.6	–2.7
R42	not located	–141.6	40.5	61.6	89.6	–12.0	–0.124	0.874	–7.4	–4.9	192.4	34.0
R43	not located	–133.3	32.9	65.8	90.7	–11.1	–0.144	0.910	–6.5	–5.6	190.5	20.7
R44	not located	–131.4	36.7	66.3	90.3	–12.3	–0.145	0.893	–6.3	–5.1	181.7	29.7
R45	not located	–148.9	38.9	57.1	88.3	–10.6	–0.134	0.841	–8.4	–5.6	214.6	27.1
R46	not located	–145.4	39.3	69.7	89.7	–9.1	–0.151	0.836	–6.8	–5.4	203.9	30.0
R47	66.4	–97.5	14.4	58.9	92.0	–16.1	0.079	0.880	–5.6	–7.0	167.2	–20.3
R48	76.9	–78.3	11.4	64.3	88.3	–16.8	–0.019	0.820	–4.4	–7.2	140.7	–19.7
R49	64.5	–91.6	15.6	65.1	90.8	–13.3	–0.001	0.858	–5.2	–6.6	150.7	–9.5
R50	not located	–106.2	26.9	75.5	88.5	–3.8	–0.217	0.765	–5.9	–5.9	154.1	17.4
R51	54.5	–98.3	23.3	69.5	88.0	–5.6	–0.212	0.729	–5.5	–6.2	144.3	12.5
R52	46.6	–111.0	20.5	84.1	87.5	3.5	–0.212	0.993	–5.4	–5.9	157.5	2.2
R53	47.0	–102.9	24.7	64.2	83.2	–6.5	–0.187	0.762	–5.7	–6.0	149.6	14.1
R54	not located	–104.4	28.4	64.3	83.9	–6.4	–0.186	0.732	–5.7	–5.7	149.5	21.1
R55	51.5	–104.7	29.5	66.9	82.8	–6.6	–0.185	0.686	–5.7	–5.7	150.7	22.9
R56	not located	–112.7	30.6	66.7	84.3	–5.5	–0.184	0.755	–6.2	–5.7	161.7	22.7
R57	not located	–114.4	30.7	64.2	83.6	–6.4	–0.177	0.767	–6.3	–5.7	163.5	22.5
R58	not located	–111.0	29.2	64.2	83.2	–6.2	–0.182	0.755	–6.1	–5.8	158.8	20.8
R59	not located	–106.8	26.5	64.2	83.5	–6.3	–0.185	0.766	–6.1	–6.0	159.0	15.5
R60	not located	–112.5	30.2	64.3	83.3	–6.6	–0.181	0.758	–6.1	–5.7	159.4	22.5
R61	51.4	–96.1	26.6	65.3	85.4	–5.6	–0.200	0.701	–5.2	–5.7	138.9	20.2
R62	not located	–113.1	29.4	63.2	84.3	–6.6	–0.140	0.757	–6.4	–5.8	164.8	19.9

R63	not located	–114.1	29.8	64.1	83.7	–6.2	–0.184	0.771	–6.4	–5.8	165.9	20.4
R64	not located	–114.0	33.8	63.1	85.0	–5.6	–0.138	0.752	–6.1	–5.4	159.7	28.6
R65	not located	–112.7	34.4	65.8	83.0	–7.7	–0.130	0.679	–6.1	–5.4	158.9	29.6
R66	50.1	–105.2	23.5	63.4	83.9	–6.0	–0.174	0.763	–6.0	–6.3	157.1	9.4
R67	62.6	–104.3	22.6	70.9	90.2	–13.3	–0.008	0.839	–5.8	–6.0	164.2	5.3
R68	not located	–115.5	32.7	70.6	86.2	–7.0	–0.205	0.765	–6.5	–5.5	167.5	25.3
R69	not located	–112.7	30.8	66.6	86.3	–9.7	–0.224	0.766	–6.2	–4.0	161.2	23.2
R70	not located	–125.3	43.4	65.9	80.2	–7.7	–0.267	0.664	–6.7	–4.8	175.3	40.8
R71	not located	–127.7	47.8	66.1	80.3	–9.4	–0.272	0.647	–6.6	–4.5	172.0	46.9
R72	not located	–132.2	46.7	62.0	77.7	–7.4	–0.225	0.666	–7.2	–4.8	183.5	44.4
R73	not located	–122.3	30.0	64.1	84.5	–5.3	–0.317	0.772	–7.1	–5.8	181.9	17.0
R74	not located	–108.2	31.1	57.6	80.3	–4.1	–0.318	0.666	–6.0	–5.6	155.7	24.7
R75	47.3	–108.2	31.9	61.8	80.9	–5.1	–0.328	0.662	–5.9	–5.5	154.5	26.3
R76	not located	–113.3	35.1	57.6	80.3	–4.3	–0.315	0.661	–6.0	–5.3	157.6	30.9
R77	56.0	–97.0	26.1	70.0	83.8	–9.2	–0.076	0.650	–5.3	–5.7	145.4	17.9
R78	not located	–121.3	44.0	70.7	80.8	–10.4	–0.285	0.671	–6.2	–4.7	164.1	42.7
R79	not located	–116.4	37.9	77.1	84.8	–12.0	–0.226	0.758	–6.1	–3.4	161.3	34.6
R80	not located	–106.6	31.0	72.8	84.6	–10.7	–0.202	0.729	–5.7	–5.5	150.8	25.5
R81	52.1	–108.1	30.2	69.2	85.3	–11.3	–0.190	0.770	–5.9	–5.6	156.2	23.2
R82	48.6	–104.5	29.3	45.8	81.8	–6.7	0.169	0.020	–5.8	–5.7	150.9	22.6
R83	not located	–129.8	49.4	79.0	86.8	–13.7	–0.210	0.717	–6.0	–4.5	172.9	48.6
R84	not located	–126.3	46.4	76.1	85.4	–12.3	–0.216	0.760	–6.5	–3.2	171.4	45.0
R85	48.3	–111.8	34.2	66.8	85.8	–10.7	–0.217	0.731	–5.9	–4.2	155.4	29.9
R86	52.7	–104.1	15.0	73.8	93.0	–4.8	0.143	0.958	–5.9	–7.0	164.6	–16.9
R87	not located	–117.9	21.5	79.5	92.5	–4.4	0.131	0.960	–6.7	–6.5	179.2	–2.5
R88	not located	–134.6	36.9	75.5	85.4	–3.0	0.107	0.813	–6.9	–5.1	183.0	29.7
R89	not located	–123.6	28.4	79.2	88.9	–3.8	0.089	0.862	–6.1	–5.6	177.9	14.8
R90	not located	–124.8	33.7	79.7	88.3	–3.5	0.088	0.828	–6.0	–5.1	172.1	26.2
R91	not located	–137.9	34.7	71.8	84.7	–2.9	0.120	0.795	–7.7	–5.7	198.3	22.6
R92	not located	–134.9	34.5	82.6	85.4	1.3	0.120	0.804	–7.2	–5.6	189.9	24.1
R93	not located	–133.4	35.2	90.3	84.4	12.0	0.101	0.815	–6.9	–5.5	184.0	26.6
R94	73.4	–75.0	10.8	77.5	87.3	–2.2	0.234	0.794	–4.1	–7.1	132.9	–18.4
R95	63.9	–98.5	16.7	79.1	91.1	–8.7	0.234	0.886	–5.0	–6.6	153.3	–7.1
R96	65.8	–92.1	13.5	72.7	91.4	–10.4	0.299	0.846	–5.1	–6.9	155.9	–18.6
R97	47.5	–101.8	23.5	86.5	89.5	6.6	0.059	0.802	–5.6	–6.0	147.4	12.1
R98	34.1	–109.4	18.2	96.0	90.0	19.8	0.007	1.010	–5.8	–6.3	155.0	–3.2
R99	48.9	–101.2	20.0	84.4	86.0	5.2	0.040	0.894	–5.4	–6.3	146.5	4.3

R100	31.2	–108.2	18.6	94.8	67.9	23.7	0.036	0.983	–5.7	–6.0	155.3	–2.3
R101	47.3	–99.0	23.1	77.5	83.3	0.6	0.079	0.745	–5.4	–6.1	143.8	12.2
R102	39.0	–106.8	26.5	79.1	87.3	–1.1	0.081	0.772	–5.9	–5.8	153.5	16.8
R103	46.0	–109.5	28.6	77.5	83.2	1.3	0.085	0.746	–5.9	–5.7	156.3	20.1
R104	44.0	–106.7	27.4	77.5	83.1	1.4	0.084	0.736	–5.8	–5.8	152.4	18.7
R105	43.3	–102.7	24.8	77.5	83.4	1.0	0.083	0.747	–5.8	–6.0	152.3	13.6
R106	43.7	–108.1	28.3	77.5	83.1	1.3	0.085	0.740	–5.8	–5.7	153.1	20.3
R107	not located	–121.7	44.1	77.6	81.6	2.7	0.090	0.692	–6.4	–4.7	168.8	42.4
R108	56.3	–84.8	17.5	77.5	82.6	–0.5	0.071	0.723	–4.7	–6.2	128.9	3.6
R109	50.2	–101.4	27.0	77.5	82.9	2.0	0.077	0.718	–5.5	–5.7	144.9	19.7
R110	53.2	–99.7	26.8	79.3	85.3	–0.2	0.081	0.687	–5.5	–5.8	143.8	19.5
R111	43.7	–107.9	27.3	76.7	82.7	1.4	0.125	0.735	–6.0	–5.8	157.1	17.5
R112	44.2	–109.0	27.7	77.4	83.1	1.9	0.080	0.747	–6.0	–5.8	158.2	18.1
R113	44.6	–115.9	31.7	77.4	83.2	2.2	0.096	0.753	–6.3	–5.6	165.7	24.0
R114	not located	–108.2	31.3	76.8	81.8	0.3	0.121	0.714	–5.8	–5.5	152.0	25.7
R115	not located	–107.8	32.5	78.1	84.7	0.1	0.129	0.646	–5.8	–5.4	152.2	27.7
R116	47.6	–97.7	23.1	76.9	78.1	5.0	0.149	0.605	–5.6	–6.2	147.0	11.3
R117	50.3	–99.1	20.6	76.9	82.6	1.2	0.101	0.732	–5.6	–6.4	148.1	5.4
R118	46.9	–111.3	31.1	82.8	83.8	2.3	0.067	0.752	–6.2	–5.6	160.7	23.8
R119	not located	–124.2	45.5	77.9	80.5	–1.6	0.007	0.653	–6.3	–4.7	168.1	44.2
R120	not located	–130.8	52.8	83.0	76.6	–4.6	–0.032	0.658	–6.6	–4.2	175.7	52.5
R121	39.2	–114.3	35.2	84.5	81.1	0.6	–0.034	0.718	–5.7	–4.7	158.9	31.0
R122	40.0	–120.6	41.4	89.9	79.3	0.1	–0.071	0.718	–6.1	–4.4	166.1	39.0
R123	not located	–126.9	43.6	75.5	76.1	–1.5	0.067	0.660	–6.8	–5.0	176.0	40.9
R124	not located	–134.5	52.3	80.9	75.1	–2.5	0.038	0.652	–7.2	–4.5	184.3	51.5
R125	46.4	–101.1	29.8	80.9	79.6	4.6	0.003	0.691	–5.5	–5.6	144.0	24.6
R126	not located	–138.1	44.3	68.1	84.7	–9.9	0.351	0.675	–7.5	–4.8	195.8	39.6

Supplementary Table 22: Correlations between LFER parameters and conventional Physical Organic Properties for radicals.

Parameter	Correlation Method	E_{SOMO}	ω	BV(r=3)	BDE	$\Delta G_{Cu\text{-}III}$	Charge	Spin	Red.	Oxi.	VIP	VEA
R_{IP}	Pearson	0.798	–0.636	–0.525	0.593	–0.770	0.021	0.091	0.688	–0.645	–0.303	–0.650
	Spearman	0.782	–0.575	–0.526	0.515	–0.714	–0.109	0.120	0.617	–0.546	–0.387	–0.509
	Kendall	0.576	–0.417	–0.353	0.363	–0.509	–0.073	0.082	0.429	–0.397	–0.277	–0.372

5.2 MLR for Approximating R_{IP}.

Supplementary Figure 16 illustrates the optimal multivariate linear regression (MLR) model for approximating R_{IP} parameters of radicals. The R_{IP} parameters were estimated using the energy of SOMO (E_{SOMO}), buried volume (BV(r=3)), the bond dissociation energy

of the targeted C-H bond in the corresponding precursor of the radical (BDE), the affinity between radicals and Cu-II complexes ($\Delta G_{\text{Cu-III}}$), single-electron reduction potential (Red.), vertical ionization potential (VIP), and vertical electron affinity (VEA) as independent variables, along with the inclusion of a cross-term combining E_{SOMO} and BV(r=3). This MLR model achieved an Q^2 value of 0.933, MAE value of 1.9 kcal/mol and RMSE value of 2.5 kcal/mol by leave-one-out cross validation (LOO-CV).

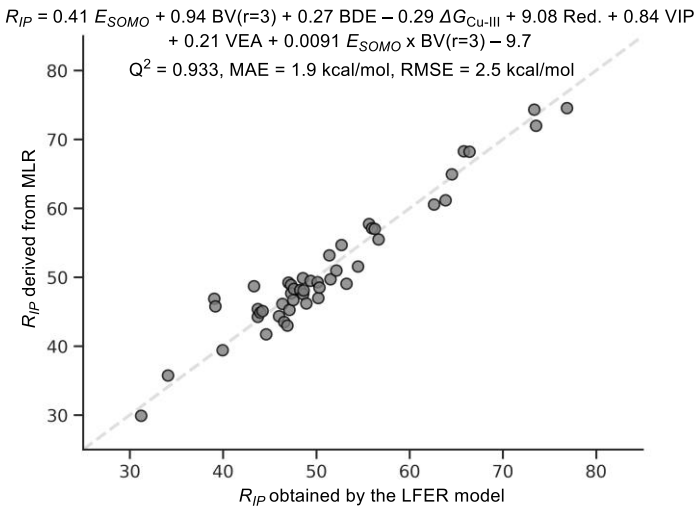

Supplementary Figure 16: Comparison of R_{IP} parameters derived from the LFER model and the MLR. Data points in this figure were obtained from the test sets of each LOO iteration.

By 5-fold cross validation, this MLR model achieved a 10-trial averaged R^2 value of 0.879, MAE value of 2.0 kcal/mol, RMSE value of 2.5 kcal/mol. Detailed code and results are provided on GitHub: https://github.com/XuGuoXiong/LFER-on-Mechanism-Prediction.git.

When building the MLR model, we considered 2047 combinations of the 11 physical organic properties listed in Supplementary Table 21 (ranging from using a single variable to using all variables), and introduced polynomial terms of these variables to improve model performance. Due to computational constraints, we limited the polynomial terms to a maximum of second order and included at most one such term per model. These 2047 models and their implementation code are provided on GitHub: https://github.com/XuGuoXiong/LFER-on-Mechanism-Prediction.git.

5.3 Linear Transformation from N_{RE} to N_{RS}.

Supplementary Figure 17 demonstrates the approximation of N_{RS} values for nucleophiles through linear transformation of N_{RE}, achieving an Q^2 value of 0.967, MAE value of 1.4 kcal/mol and RMSE value of 1.7 kcal/mol by leave-one-out cross validation (LOO-CV). However, this linear transformation is only applicable to *sp*- and sp^2-hybridized nucleophiles. Detailed code is provided on GitHub: https://github.com/XuGuoXiong/LFER-on-Mechanism-Prediction.git.

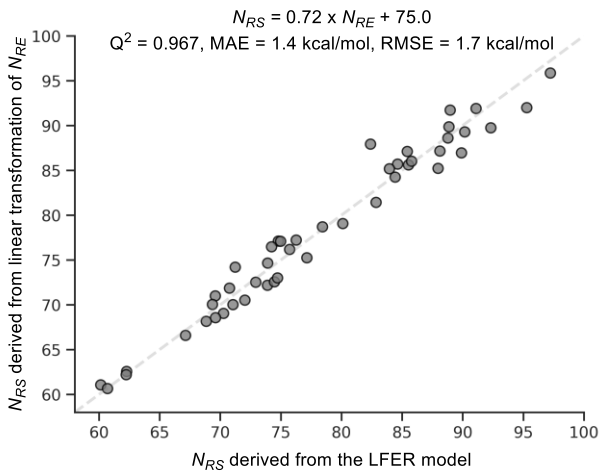

Supplementary Figure 17: Comparison of N_{IP} parameters: linear transformation vs. LFER model. Data points in this figure were obtained from the test sets of each LOO iteration.

5.4 The Comparison between LFER Parameters and Physical Organic Properties of Nucleophiles.

We identified a potential linear relationship between the N_{RE} and N_{RS} parameters for *sp*- and sp^2-hybridized nucleophiles (Supplementary Figure 17). This enables the approximation of missing N_{RS} values for *sp*- and sp^2-hybridized nucleophiles in Supplementary Table 6 and Supplementary Table 23 (due to the inability to locate RS-TS) through linear transformation of N_{RE}.

The LFER parameters for nucleophiles and their correlations with conventional Physical Organic Properties are presented in Supplementary Table 23, with the corresponding correlation analyses detailed in Supplementary Table 24.

Supplementary Table 23: The comparison between LFER parameters and conventional Physical Organic Properties of nucleophiles. E_{HOMO}**,** the energy of HOMO, values in kcal/mol. ω^-**,** electrodonating power[25], values in kcal/mol. ω**,** the global electrophilicity index[24], values in kcal/mol. **BV(r=3),** the buried volume within a 3 Å radius of the nucleophile bond formation atom center, values in %. **VIP**, vertical ionization potential, values in eV. **VEA**, vertical electron affinity, values in eV.

Nucleophiles	N_{RS}	E_{HOMO}	ω^-	ω	BV(r=3)	charge	VIP	VEA
N1	92.3	37.9	0.015	3.893	52.6	–0.215	35.4	–100.5
N2	88.8	26.5	0.809	1.776	40.1	–0.415	41.0	–83.0
N3	not located	10.0	5.298	0.137	52.6	–0.170	57.9	–69.8
N4	74.8	0.2	9.734	0.125	40.1	–0.366	60.1	–49.7
N5	95.3	34.0	0.359	2.198	52.5	–0.211	35.5	–80.8
N6	91.1	26.1	1.272	1.108	40.1	–0.416	39.2	–70.4
N7	73.9	–7.0	7.187	0.087	30.2	–0.530	71.6	–82.0
N10	67.1	–19.5	8.799	0.074	30.2	–0.507	84.7	–95.0
N11	71.0	–6.5	6.517	0.148	29.9	–0.515	70.0	–83.5
N12	62.3	12.5	5.176	1.235	22.1	–0.461	94.2	–142.5
N13	82.9	19.5	3.546	0.991	29.3	–0.584	68.1	–105.2
N14	74.5	–8.9	8.961	0.002	30.2	–0.526	69.3	–67.7

N15	72.9	–9.9	6.911	0.101	35.2	–0.549	70.3	–81.4
N16	69.6	–20.4	9.255	0.000	47.2	–0.496	73.4	–73.0
N17	69.3	–15.0	8.992	0.008	31.7	–0.504	76.7	–79.9
N18	68.8	–16.7	9.573	0.002	30.3	–0.509	78.7	–80.1
N19	70.3	–15.2	8.872	0.011	30.2	–0.513	76.3	–80.0
N20	72.0	–8.7	7.458	0.088	30.2	–0.528	74.2	–84.8
N21	69.6	–17.1	10.465	0.012	30.2	–0.509	77.7	–73.8
N24	60.1	–36.0	24.331	1.921	30.3	–0.458	94.0	–47.4
N25	77.1	–6.0	7.642	0.010	30.3	–0.531	66.0	–69.3
N26	62.2	–24.1	14.957	0.204	31.4	–0.480	91.7	–75.2
N27	60.7	–16.8	10.935	0.086	30.0	–0.508	104.6	–116.9
N28	74.7	–9.0	10.985	0.010	30.8	–0.399	82.4	–78.9
N29	88.9	24.2	0.806	1.754	44.9	–0.451	40.6	–82.2
N30	89.0	32.6	0.112	2.740	54.7	–0.175	32.2	–82.3
N31	not located	26.9	0.737	1.792	44.5	–0.414	39.7	–81.4
N32	82.4	17.4	1.532	1.048	55.1	–0.393	42.2	–73.3
N33	90.2	24.5	1.561	0.929	40.1	–0.413	40.3	–68.8
N34	88.1	19.9	1.464	1.277	40.5	–0.399	45.1	–81.0
N35	84.4	18.1	1.669	1.186	40.2	–0.401	46.7	–81.6
N36	85.5	19.0	1.559	1.230	40.2	–0.403	45.8	–81.2
N37	85.4	24.4	1.004	1.697	40.2	–0.414	43.8	–85.7
N38	84.6	17.2	2.196	0.817	40.2	–0.400	46.8	–75.0
N39	97.2	52.9	0.186	5.755	38.3	–0.455	30.0	–110.3
N40	not located	31.9	0.112	3.121	60.9	–0.284	35.9	–92.5
N43	not located	15.1	0.616	1.845	78.8	–0.272	37.8	–79.4
N44	not located	32.8	0.458	1.990	52.4	–0.209	35.8	–78.4
N45	not located	7.6	2.273	1.174	56.1	–0.153	55.3	–92.6
N46	not located	20.9	0.731	2.233	53.0	–0.182	45.4	–95.6
N47	not located	25.6	0.687	2.240	52.6	–0.195	44.5	–94.4
N48	not located	32.4	0.236	3.157	52.6	–0.210	41.8	–102.1
N49	not located	22.0	1.231	1.621	52.6	–0.188	46.8	–88.7
N50	84.0	24.5	0.835	1.753	52.6	–0.193	41.2	–83.0
N51	not located	22.8	0.863	1.805	56.3	–0.243	42.5	–85.5
N52	74.2	15.8	1.866	1.472	52.2	–0.191	54.8	–97.1
N53	80.1	14.7	1.680	1.579	52.6	–0.183	53.7	–97.4
N54	73.9	1.4	3.571	0.794	55.6	–0.157	63.5	–95.3
N55	75.0	24.1	1.142	2.080	52.2	–0.207	51.9	–102.6

N56	71.2	7.9	3.317	0.753	52.3	−0.177	59.4	−89.3
N57	88.0	20.7	1.320	1.672	49.4	−0.132	49.2	−92.7
N58	89.9	28.8	0.494	2.463	49.5	−0.141	42.4	−94.3
N59	85.8	23.7	0.591	2.343	50.0	−0.123	43.5	−94.3
N61	not located	31.0	0.402	2.189	49.5	−0.155	36.6	−82.3
N62	not located	28.5	0.540	2.049	53.2	−0.178	38.6	−83.2
N63	78.4	6.8	3.133	0.818	51.6	−0.158	58.8	−90.0
N64	not located	8.6	2.865	0.835	56.1	−0.131	55.9	−86.7
N65	70.7	−8.5	5.690	0.352	51.3	−0.325	72.3	−94.0
N66	75.7	−1.3	5.815	0.229	50.9	−0.360	67.9	−84.6
N67	76.3	−2.6	6.847	0.128	51.2	−0.343	71.7	−84.4
N68	not located	86.7	2.625	11.271	25.6	−0.767	18.9	−137.6
N69	not located	72.9	4.811	12.245	57.0	−0.264	6.2	−115.3
N70	not located	64.4	3.792	10.956	71.2	−0.020	8.6	−111.0
N71	not located	34.0	1.769	3.002	47.2	0.359	77.3	−151.4
N72	not located	40.1	0.619	6.124	48.9	−0.573	20.9	−96.9
N73	not located	37.2	0.923	6.281	77.4	0.010	16.8	−90.0
N74	not located	34.6	0.199	4.326	48.9	−0.571	20.4	−79.2
N75	not located	33.8	0.244	5.020	56.6	−0.580	23.3	−91.1
N72	not located	28.5	0.014	4.217	51.6	−0.565	29.7	−94.4
N73	not located	27.6	0.003	4.013	49.0	−0.562	30.3	−93.3
N74	not located	29.5	0.070	4.532	49.0	−0.567	27.3	−93.4
N75	not located	38.8	0.446	5.801	48.9	−0.577	22.7	−97.3
N73	not located	26.8	0.001	3.756	49.0	−0.565	29.1	−88.6
N74	not located	−0.8	3.219	0.698	49.2	−0.523	56.8	−84.9
N75	not located	34.7	0.191	4.447	48.9	−0.571	21.5	−82.2

Supplementary Table 24: Correlation results between LFER parameters and conventional Physical Organic Properties of nucleophiles.

Parameter	Correlation Method	E_{HOMO}	ω^-	ω	BV(r=3)	charge	VIP	VEA
N_{RS}	Pearson	0.892	−0.806	0.668	0.479	0.397	−0.938	0.009
	Spearman	0.916	−0.864	0.683	0.474	0.443	−0.937	−0.067
	Kendall	0.769	−0.688	0.525	0.302	0.214	−0.806	−0.051

6 Contributions of Different Components.

The numerical range of LFER parameters for different reaction components reflects their relative influence on the free energy changes of bond formation processes. A larger numerical range of the LFER parameter for a specific component indicates a greater contribution of

that component to the bond formation process, suggesting that variations in this component significantly impact the free energy changes. Conversely, a smaller numerical range implies a lesser influence.

Supplementary Figure 18 presents a box plot illustrating the distribution of LFER parameters. The upper and lower edges of the box represent the upper quartile (Q3) and lower quartile (Q1), respectively, while the horizontal line within the box denotes the median (Q2). The cross symbol inside the box indicates the mean value. The whiskers extending from the box reflect the data spread, with longer whiskers indicating a wider data range and shorter whiskers suggesting a more concentrated distribution. Individual data points for each reaction component are represented by circles.

The results reveal that, across the three bond formation processes, the LFER parameters for ligands and nucleophiles exhibit broader numerical ranges compared to those for radicals, with ligands showing a slightly wider range than nucleophiles. In contrast, the LFER parameters for radicals are concentrated within a narrower range. These findings indicate that, within the chemical space explored in this study, ligands and nucleophiles exert a more significant influence on the bond formation processes, whereas radicals play a relatively minor role.

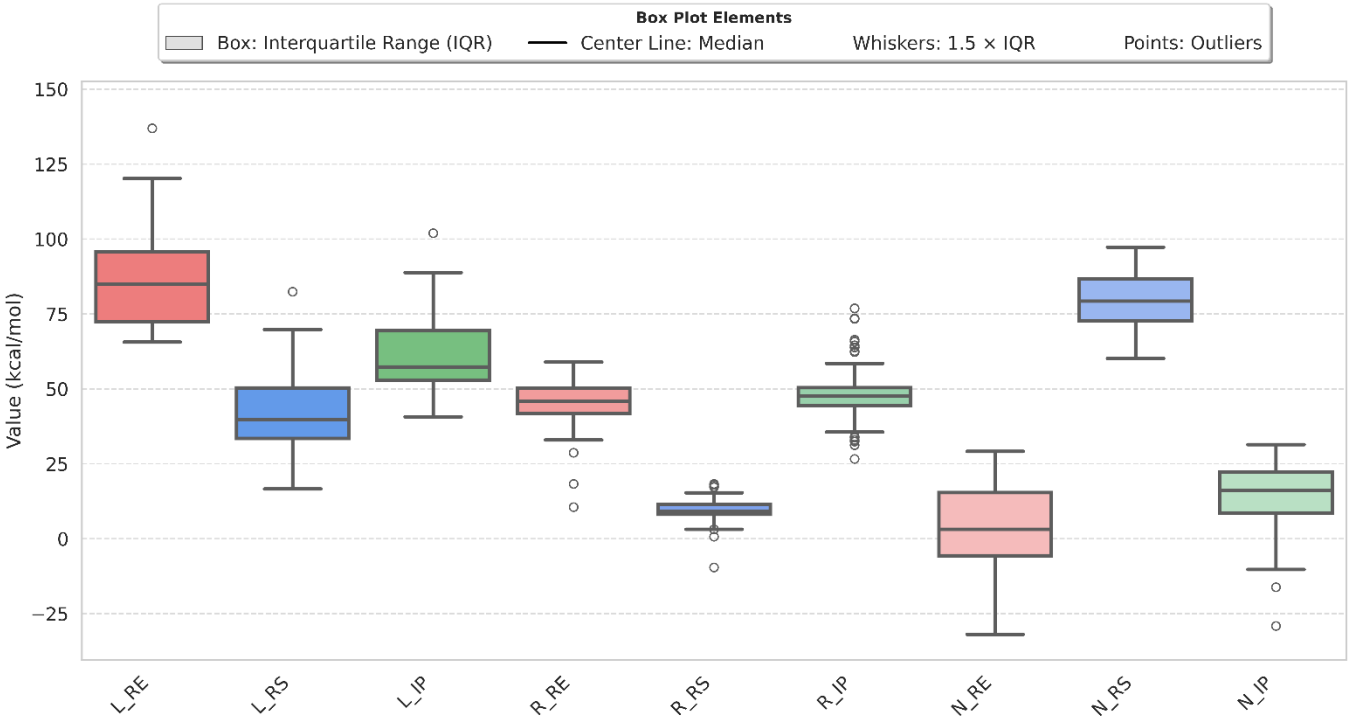

Supplementary Figure 18: Range of LFER parameters of ligands, radicals and nucleophiles.

7 Application in Actual Catalytic Reactions.

Using our established LFER model, we can predict the favored bond formation mechanisms for various ligand-radical-nucleophile combinations. Here, we assume that modifications to substituents (e.g., introducing chiral groups) on the same ligand scaffold do not significantly alter the mechanistic selectivity of the combinations. In Supplementary Figure 19, we present the chemical structures of the ligands and radical coupling products used in the actual catalytic reaction systems, the additional coordinating atoms at the copper center (if neutral ligands are employed), the favored bond formation mechanism predicted by the LFER model, and the favored mechanism determined by comprehensive DFT calculations. These combinations were derived from previously reported DFT computational studies on copper-catalyzed radical transformations, which specifically investigated the bond formation processes[26-35].

Considering potential variations in theoretical levels across these studies, we systematically re-evaluated the transition state structures

and energetics for each bond formation process at the B3LYP-D3(BJ)/6-311+G(d,p)-SDD-SMD(Solvent)//B3LYP-D3(BJ)/6-31G(d)-LANL2DZ level of theory to ensure computational consistency.

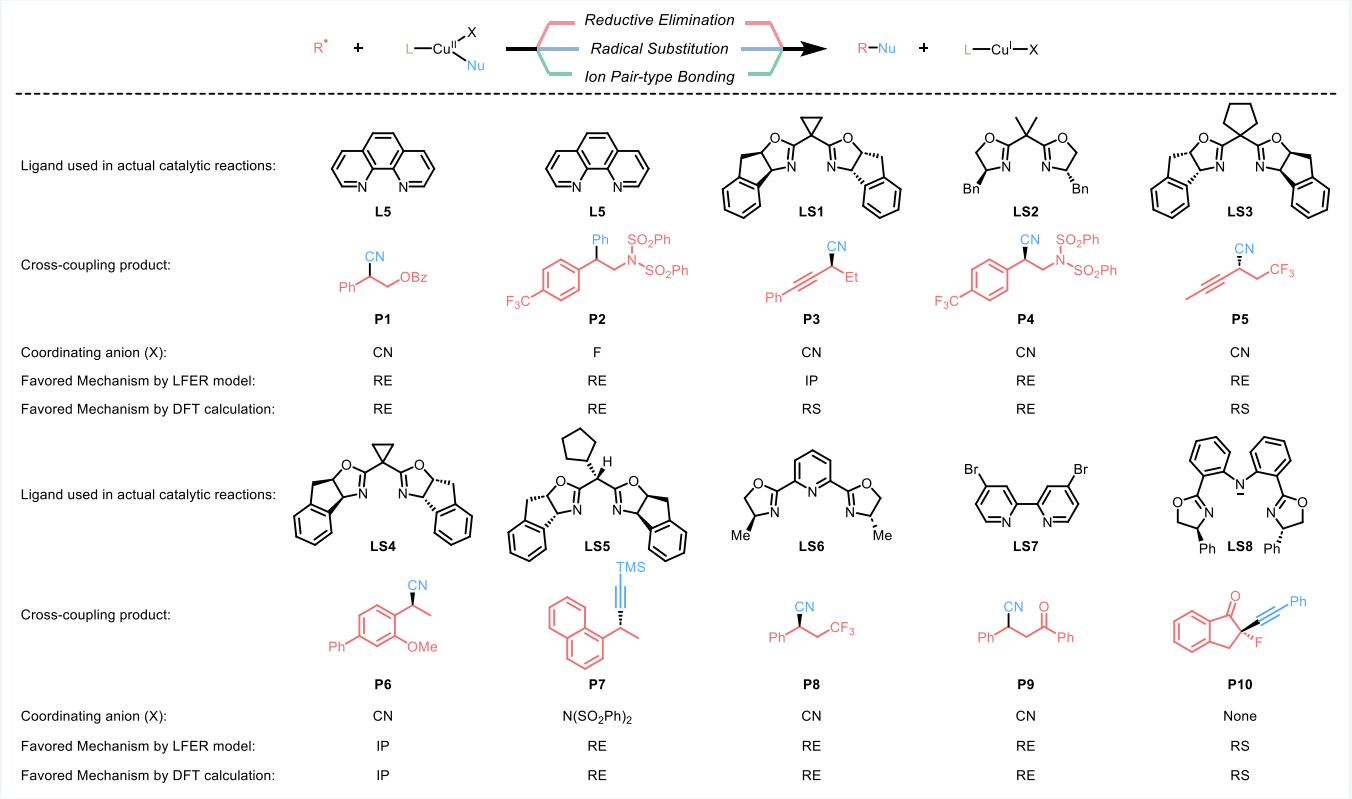

Supplementary Figure 19: Application of the LFER predictive model to actual catalytic reactions.

Supplementary Table 25 summarizes the statistics of transformations presented in Supplementary Figure 19. The table comprises: (i) the predicted free energy changes ($\Delta G^{\ddagger}_{RE}$(pred.), $\Delta G^{\ddagger}_{RS}$(pred.), and $\Delta G^{\ddagger}_{IP}$(pred.)) obtained from the LFER model; (ii) the free energy difference ($\Delta\Delta G^{\ddagger}$) obtained by the LFER prediction and DFT calculations, defined as the difference between the free energy of the respective transition states and that of the reductive elimination transition state; and (iii) the predicted favored mechanism and the confirmed favored mechanism validated by DFT calculations.

Supplementary Table 25: Details of LFER prediction and DFT calculation in Supplementary Figure 19.

Ligand	Product	$\Delta G^{\ddagger}_{RE}$ (pred.)	$\Delta G^{\ddagger}_{RS}$ (pred.)	$\Delta G^{\ddagger}_{IP}$ (pred.)	LFER-Predicted		DFT-Calculated		Predicted Mechanism	Calculated Mechanism
					$\Delta\Delta G^{\ddagger}$ (RS-RE)	$\Delta\Delta G^{\ddagger}$ (IP-RE)	$\Delta\Delta G^{\ddagger}$ (RS-RE)	$\Delta\Delta G^{\ddagger}$ (IP-RE)		
L5	**P1**	–118.5	–111.9	–113.4	6.6	5.1	0.3	not located	RE	RE
L5	**P2**	–158.3	–146.3	–129.9	12.0	28.3	10.3	not located	RE	RE
LS1	**P3**	–105.7	–106.1	–107.0	–0.4	–1.3	–5.6	–4.5	IP	RS
LS2	**P4**	–114.0	–112.1	–103.3	1.9	10.7	2.6	not located	RE	RE
LS3	**P5**	–106.9	–100.5	–104.2	6.5	1.8	–0.1	5.9	RE	RS
LS4	**P6**	–110.0	–106.3	–111.1	3.7	–1.1	0.2	–1.3	IP	IP
LS5	**P7**	–122.3	–121.6	–122.2	0.7	0.1	1.2	not located	RE	RE

LS6	**P8**	–95.9	–88.1	–92.1	7.8	3.8	8.4	not located	RE	RE
LS7	**P9**	–115.7	–114.1	–113.8	1.6	1.8	4.6	3.6	RE	RE
LS8	**P10**	–108.6	–121.4	–99.8	–12.8	8.8	–4.2	not located	RS	RS

Supplementary Table 26 summarizes the mechanistic selectivity variations of these transformations in the reaction solvents reported in the corresponding literature. Consistent with our conclusions in Section 3.3, the LFER predictive model demonstrates reliable applicability for nonpolar and low-polarity solvents. However, in highly polar solvents, the model's predictive validity is restricted exclusively to combinations exhibiting singularly dominant mechanistic selectivity.

Supplementary Table 26: Application of the LFER predictive model in actual solvents.

Ligand	Product	Solvent	Predicted		Calculated (in gas)		Calculated (in solvent)		Predicted Mechanism	Calculated Mechanism	
			$\Delta\Delta G^{\ddagger}$ (RS-RE)	$\Delta\Delta G^{\ddagger}$ (IP-RE)	$\Delta\Delta G^{\ddagger}$ (RS-RE)	$\Delta\Delta G^{\ddagger}$ (IP-RE)	$\Delta\Delta G^{\ddagger}$ (RS-RE)	$\Delta\Delta G^{\ddagger}$ (IP-RE)		in gas	in solvent
L5	**P1**	THF	6.6	5.1	0.3	not located	–0.6	not located	RE	RE	RS
L5	**P2**	DCM	12.0	28.3	10.3	not located	10.3	not located	RE	RE	RE
LS1	**P3**	MeCN	–0.4	–1.3	–5.6	–4.5	–1.3	6.0	IP	RS	RS
LS2	**P4**	DMA	1.9	10.7	2.6	not located	–1.0	not located	RE	RE	RS
LS3	**P5**	PhCl	6.5	1.8	–0.1	5.9	–2.9	5.4	RE	RS	RS
LS4	**P6**	MeCN	3.7	–1.1	0.2	–1.3	–1.3	6.0	IP	IP	RS
LS5	**P7**	TFEA	0.7	0.1	1.2	not located	0.3	not located	RE	RE	RE
LS6	**P8**	DCM	7.8	3.8	8.4	not located	6.9	not located	RE	RE	RE
LS7	**P9**	cyclohexane	1.6	1.8	4.6	3.6	4.6	6.3	RE	RE	RE
LS8	**P10**	MeCN	–12.8	8.8	–4.2	not located	–5.2	not located	RS	RS	RS

In the reactions we selected for evaluation in Supplementary Figure 19 were primarily cases where the mechanism had already been studied in detail by other groups using DFT. This was intended to provide an independent and fair assessment of our model's predictive reliability. However, this selection criterion inadvertently led to a dataset dominated by RE pathways, which in turn inflated the baseline accuracy and limited the extent to which the predictive advantage of our model could be clearly demonstrated.

So, we expanded the distribution of RS and IP pathways in the reactions for evaluation, thereby providing a more balanced and rigorous evaluation of the LFER model. Specifically, we added 10 new reactions that our LFER model predicts to proceed via either the RS or IP pathway (Supplementary Figure 20). These additional cases involve 7 distinct ligands, 9 radicals, and 9 nucleophiles, thus posing a substantial challenge in terms of structural diversity. Comparison of the model predictions with DFT validation shows that the model correctly identified the operative pathway in 9 out of 10 cases.

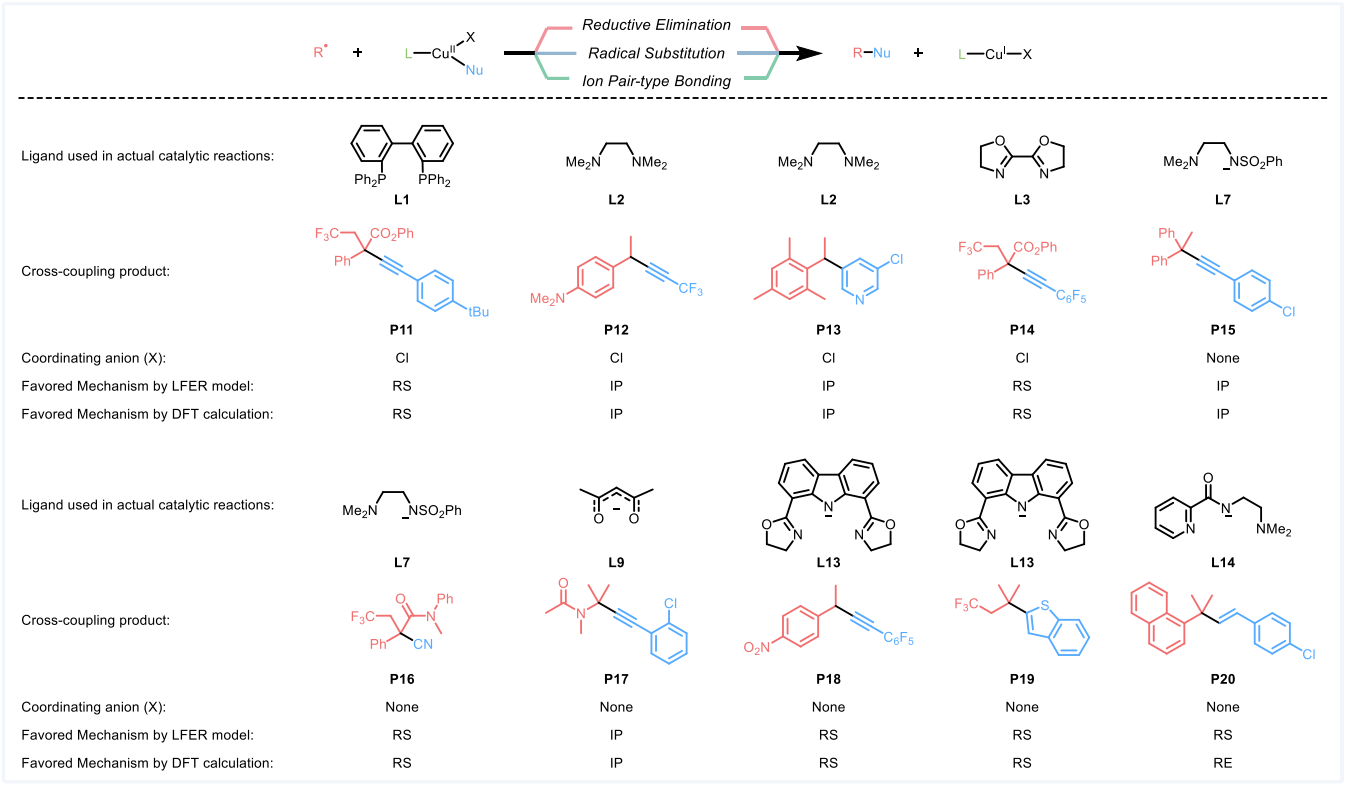

Supplementary Figure 20: Application of the LFER predictive model to additional reaction combinations.

Supplementary Table 27 summarizes the statistics of transformations presented in Supplementary Figure 20. The table comprises: (i) the predicted free energy changes ($\Delta G^{\ddagger}_{RE}$(pred.), $\Delta G^{\ddagger}_{RS}$(pred.), and $\Delta G^{\ddagger}_{IP}$(pred.)) obtained from the LFER model; (ii) the free energy difference ($\Delta\Delta G^{\ddagger}$) obtained by the LFER prediction and DFT calculations, defined as the difference between the free energy of the respective transition states and that of the reductive elimination transition state; and (iii) the predicted favored mechanism and the confirmed favored mechanism validated by DFT calculation.

Supplementary Table 27: Details of LFER prediction and DFT calculation in Supplementary Figure 20.

Ligand	Product	$\Delta G^{\ddagger}_{RE}$ (pred.)	$\Delta G^{\ddagger}_{RS}$ (pred.)	$\Delta G^{\ddagger}_{IP}$ (pred.)	LFER-Predicted $\Delta\Delta G^{\ddagger}$ (RS-RE)	LFER-Predicted $\Delta\Delta G^{\ddagger}$ (IP-RE)	DFT-Calculated $\Delta\Delta G^{\ddagger}$ (RS-RE)	DFT-Calculated $\Delta\Delta G^{\ddagger}$ (IP-RE)	Predicted Mechanism	Calculated Mechanism
L1	**P11**	–105.4	–109.1	–102.1	–3.7	3.3	–4.8	not located	RS	RS
L2	**P12**	–113.9	–108.5	–123.1	5.4	–9.2	2.6	–8.4	IP	IP
L2	**P13**	–126.0	–128.1	–133.1	–2.1	–7.1	–3.8	–5.7	IP	IP
L3	**P14**	–103.8	–112.1	–110.8	–4.0	8.1	–8.8	7.8	RS	RS
L7	**P15**	–141.3	–139.8	–145.0	1.5	–3.7	–0.2	–6.8	IP	IP
L7	**P16**	–128.1	–132.6	–129.5	–4.5	–1.4	–5.0	–3.8	RS	RS
L9	**P17**	–176.6	unfavored	–182.2	unfavored	–5.6	not located	–6.3	IP	IP
L13	**P18**	–109.9	–116.4	–103.1	–6.5	6.8	–2.2	4.0	RS	RS
L13	**P19**	–92.5	–106.9	–89.3	–14.4	3.2	–8.0	not located	RS	RS
L14	**P20**	–144.8	–150.1	–132.1	–5.3	12.7	1.5	not located	RS	RE

8 Supplementary References.

1. Frisch, M.J., Trucks, G.W., Schlegel, H.B., Scuseria, G.E., Robb, M.A., Cheeseman, J.R., Scalmani, G., Barone, V., Petersson, G.A., Nakatsuji, H., Li, X., Caricato, M., Marenich, A.V., Bloino, J., Janesko, B.G., Gomperts, R., Mennucci, B., Hratchian, H.P., Ortiz, J.V., Izmaylov, A.F., Sonnenberg, J.L., Williams-Young, D., Ding, F., Lipparini, F., Egidi, F., Goings, J., Peng, B., Petrone, A., Henderson, T., Ranasinghe, D., Zakrzewski, V.G., Gao, J., Rega, N., Zheng, G., Liang, W., Hada, M., Ehara, M., Toyota, K., Fukuda, R., Hasegawa, J., Ishida, M., Nakajima, T., Honda, Y., Kitao, O., Nakai, H., Vreven, T., Throssell, K., Montgomery, J.A.Jr., Peralta, J.E., Ogliaro, F., Bearpark, M.J., Heyd, J.J., Brothers, E.N., Kudin, K.N., Staroverov, V.N., Keith, T.A., Kobayashi, R., Normand, J., Raghavachari, K., Rendell, A.P., Burant, J.C., Iyengar, S.S., Tomasi, J., Cossi, M., Millam, J.M., Klene, M., Adamo, C., Cammi, R., Ochterski, J.W., Martin, R.L., Morokuma, K., Farkas, O., Foresman, J.B. and Fox, D.J. (2016). Gaussian 16, Revision A.03.
2. Lee, C., Yang, W. & Parr, R.G. Development of the Colle-Salvetti correlation-energy formula into a functional of the electron density. *Phys. Rev. B* **37**, 785–789 (1988).
3. Becke, A.D. Density-functional thermochemistry. III. The role of exact exchange. *J. Chem. Phys.* **98**, 5648–5652 (1993).
4. Grimme, S., Antony, J., Ehrlich, S. & Krieg, H. A consistent and accurate *ab initio* parametrization of density functional dispersion correction (DFT-D) for the 94 elements H-Pu. *J. Chem. Phys.* **132**, 154104 (2010).
5. Grimme, S., Ehrlich, S., & Goerigk, L. Effect of the damping function in dispersion corrected density functional theory. *J. Comput. Chem.* **32**, 1456–1465 (2011).
6. Dunning Jr., T.H. & Hay, P.J. Gaussian Basis Sets for Molecular Calculations. In Modern Theoretical Chemistry, H.F. Schaefer, ed. (Plenum, New York), pp. 1–27 (1997).
7. Hay, P.J., & Wadt, W.R. *Ab initio* effective core potentials for molecular calculations. Potentials for the transition metal atoms Sc to Hg. *J. Chem. Phys.* **82**, 270–283 (1985).
8. Wadt, W.R. & Hay, P.J. *Ab initio* effective core potentials for molecular calculations. Potentials for main group elements Na to Bi. *J. Chem. Phys.* **82**, 284–298 (1985).
9. Hay, P. J. & Wadt, W. R. *Ab initio* effective core potentials for molecular calculations. Potentials for K to Au including the outermost core orbitals. *J. Chem. Phys.* **82**, 299–310 (1985).
10. Häussermann, U. *et al.* Accuracy of energy-adjusted quasirelativistic *ab initio* pseudopotentials: All-electron and pseudopotential benchmark calculations for Hg, HgH and their cations. *Molecular Physics* **78**, 1211–1224 (1993).
11. Igel-Mann, G., Stoll, H. & Preuss, H. Pseudopotentials for main group elements (IIIa through VIIa). *Molecular Physics* **65**, 1321–1328 (1988).
12. Bergner, A., Dolg, M., Küchle, W., Stoll, H. & Preuß, H. *Ab initio* energy-adjusted pseudopotentials for elements of groups 13–17. *Mol. Phys.* **80**, 1431–1441 (1993).
13. Marenich, A.V., Cramer, C.J. & Truhlar, D.G. Universal Solvation Model Based on Solute Electron Density and on a Continuum Model of the Solvent Defined by the Bulk Dielectric Constant and Atomic Surface Tensions. *J. Phys. Chem. B* **113**, 6378–6396 (2009).
14. Saitow, M., Becker, U., Riplinger, C., Valeev, E. F., Neese, F., A New Near-linear Scaling, Efficient and Accurate, Open-shell Domain-based Local Pair Natural Orbital Coupled Cluster Singles and Doubles Theory. *J. Chem. Phys.* **146,** 164105 (2017)
15. Neese, F. The ORCA program system, Wiley Interdisciplinary Reviews: Computational Molecular Science, 2012, Vol. 2, Issue 1, Pages 73–78;
16. Neese, F. Software update: the ORCA program system, version 4.0 Wiley Interdisciplinary Reviews: Computational Molecular Science, 2017, Vol. 8, Issue 1, p. e1327
17. Weigend , F. & Ahlrichs, R. Balanced Basis Sets of Split Valence, Triple Zeta Valence and Quadruple Zeta Valence Quality for H to Rn: Design and Assessment of Accuracy. *Phys. Chem. Chem. Phys.* **7,** 3297–3305 (2005)
18. Hellweg, A., Hattig, C., Hofener, S., & Klopper, W. Optimized Accurate Auxiliary Basis Sets for RI-MP2 and RI-CC2 Calculations for

the Atoms Rb to Rn. *Theor. Chem. Acc.* **117,** 587–597 (2007)
19. Canada. CYLview Visualization Software. http://www.cylview.org.
20. Liu, J.-R., Xu, G.-X., Liu, L.-G., Zhang, S.-Q. & Hong, X. Recent advances in theoretical studies on Cu-mediated bond formation mechanisms involving radicals. *ACS Catal.* **14**, 2429–2454 (2024).
21. Sigman, M. S., Harper, K. C., Bess, E. N. & Milo, A. The development of multidimensional analysis tools for asymmetric catalysis and beyond. *Acc. Chem. Res.* **49,** 1292–1301 (2016).
22. Reid, J. P. & Sigman, M. S. Comparing quantitative prediction methods for the discovery of small-molecule chiral catalysts. *Nat. Rev. Chem.* **2,** 290–305 (2018).
23. Nistanaki, S. K. *et al.* Catalytic asymmetric C–H insertion reactions of vinyl carbocations. *Science* **378**, 1085–1091 (2022).
24. De Vleeschouwer, F., Van Speybroeck, V., Waroquier, M., Geerlings, P. & De Proft, F. Electrophilicity and nucleophilicity index for radicals. *Org. Lett.* **9**, 2721–2724 (2007).
25. Gázquez, J.L., Cedillo, A. & Vela, A. Electrodonating and electroaccepting powers. *J. Phys. Chem. A* **111**, 1966–1970 (2007).
26. Jiao, Y., Chiou, M.-F., Li, Y. & Bao, H. Copper-catalyzed radical acyl-cyanation of alkenes with mechanistic studies on the tert -butoxy radical. *ACS Catal.* 9, 5191–5197 (2019).
27. Mo, X., Huang, H. & Zhang, G. Tetrasubstituted carbon stereocenters via copper-catalyzed asymmetric sonogashira coupling reactions with cyclic gem-dihaloketones and tertiary α-carbonyl bromides. *ACS Catal.* **12**, 9944–9952 (2022).
28. Wang, F. *et al.* Enantioselective copper-catalyzed intermolecular cyanotrifluoromethylation of alkenes via radical process. *J. Am. Chem. Soc.* **138**, 15547–15550 (2016).
29. Fu, L., Zhang, Z., Chen, P., Lin, Z. & Liu, G. Enantioselective copper-catalyzed alkynylation of benzylic C–H bonds via radical relay. *J. Am. Chem. Soc.* **142**, 12493–12500 (2020).
30. Zhang, B. et al. Enantioselective cyanofunctionalization of aromatic alkenes via radical anions. *J. Am. Chem. Soc.* **146**, 1410–1422 (2024).
31. Wang, F. *et al.* Divergent synthesis of CF_3 -substituted allenyl nitriles by ligand-controlled radical 1,2- and 1,4-addition to 1,3-enynes. *Angew. Chem., Int. Ed.* **57**, 7140–7145 (2018).
32. Wang, D., Wang, F., Chen, P., Lin, Z. & Liu, G. Enantioselective copper-catalyzed intermolecular amino- and azidocyanation of alkenes in a radical process. *Angew. Chem., Int. Ed.* **56**, 2054–2058 (2017).
33. Lu, F.-D. *et al.* Asymmetric propargylic radical cyanation enabled by dual organophotoredox and copper catalysis. *J. Am. Chem. Soc.* **141**, 6167–6172 (2019).
34. Wang, D. *et al.* Asymmetric copper-catalyzed intermolecular aminoarylation of styrenes: efficient access to optical 2,2-diarylethylamines. *J. Am. Chem. Soc.* **139**, 6811–6814 (2017).
35. Zeng, Y., Li, Y., Lv, D. & Bao, H. Copper-catalyzed three-component oxycyanation of alkenes. *Org. Chem. Front.* **8**, 908–914 (2021).